TESLA-FEL Report 2007-05

Optics Solution for the XFEL Post-Linac Collimation Section

V.Balandin, R.Brinkmann, W.Decking, and N.Golubeva
Deutsches Elektronen-Synchrotron DESY, Hamburg, Germany

Contents

1 Introduction

The post-linac collimation system of the European X-Ray FEL Facility (XFEL) should simultaneously fulfill several different functions. In first place, during routine operations, it should remove with high efficiency off-momentum and large amplitude halo particles, which could be lost inside undulator modules and become the source of radiation-induced demagnetization of undulator permanent magnets.

The system also must protect the undulator modules and other downstream equipment against miss-steered and off-energy beams in the case of machine failure without being destroyed in the process. In order to avoid unnecessary complications, the post-linac collimation system is designed as passive (i.e. without integrated fast emergency extraction system, or fast sweeping system, or fast beam enlarging system). The collimators must be able to withstand a direct impact of such number of bunches which can be delivered to their locations until a failure will be detected and the beam production in the RF gun is switched off.

From the beam dynamics point of view, the collimation section, as a part of the beam transport line from accelerator to undulators, must meet a very tight set of performance specifications. It should be able to accept bunches with different energies (up to $\pm 1.5\%$ from nominal energy) and transport them without any noticeable deterioration not only of transverse, but also of longitudinal beam parameters, i.e. it must be sufficiently achromatic and sufficiently isochronous. This will not only reduce jitter of transverse beam parameters and time of flight jitter due to an energy jitter, but also will allow to fine-tune the FEL wavelength by changing the electron beam energy without adjusting magnet strengths (an energy change of $\pm 1\%$ corresponds to a $\pm 2\%$ change in the FEL wavelength) and, even more, will make possible to scan the FEL radiation wavelength within a bunch train by appropriate programming of the low level RF system.

Some of above requirements are not in good agreement with one another and, as often, the basic problem is to find a balance among all competing factors so as to have at the end a system which still satisfactory fulfills design goals. For example, relatively large betatron functions, which are needed at the collimator locations to guarantee their survival during occasional beam impacts, lead, as a rule, to unacceptable chromatic aberrations and, therefore, chromaticity correcting sextupoles are essential in preventing the dependence of linear optical parameters on the energy deviation. Chromatic-aberration correction with sextupoles, in the next turn, requires a beamline with dispersion, which, in the relatively short system, makes separate regulation of transverse and energy collimation depths difficult and thus reduces flexibility of a system, and so on.

The conceptual design for the XFEL post-linac collimation system which satisfactory fulfills the listed above requirements was first suggested in [1, 2] and then, with some minor modifications, was evolved into practically realizable form in [3, 4, 5, 6] and was shortly described in the XFEL Technical Design Report (TDR) [7].

The following report gives a detailed description of the XFEL post-linac collimation section together with recently made design modifications. These include among others: length rearrangement between different subsystems in order to increase optics flexibility, shortening of the length of dipole magnets from $5\,m$ to $2.5\,m$ in order to reduce number of different magnet types involved in the XFEL design, and introduction of additional small dipoles ($0.5\,m$ long) into the arcs of the collimation system for adjustment of the first-order momentum compaction.

2 System Overview

The part of the beam transport from linac to undulators, which we call the **post-linac collimation section** and which is shown in fig.1, starts from the centre of the last linac quadrupole (cold quadrupole in the last accelerating module) and ends at the centre of the first quadrupole of the downstream distribution system. It consists of two arcs (figs. 2 and 3) separated by a straight section (phase shifter, fig.5) and includes matching modules at both ends (figs. 6 and 7) to adapt the optic to the desired upstream and downstream beam behaviour.

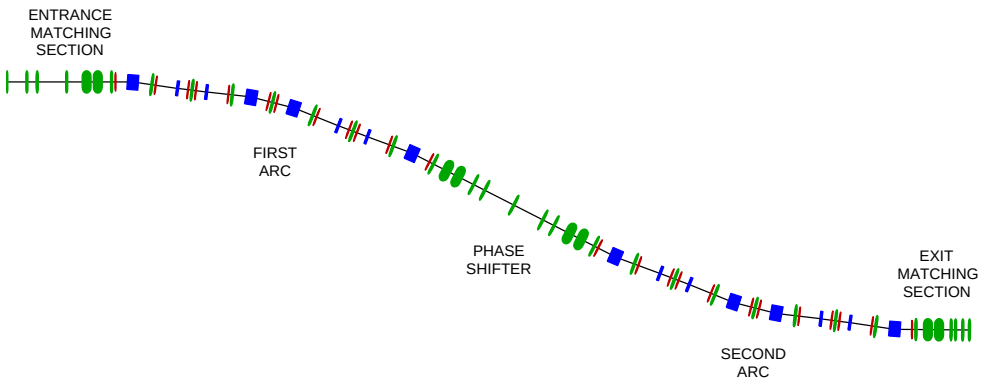

Figure 1: Overall layout of the XFEL post-linac collimation section. Blue, green and red colors mark dipole, quadrupole and sextupole magnets, respectively.

The collimation section bends the beam in the vertical plane and its length measured along the curved beam path is $215.31\,m$, while the projection on the linac axis gives $215.29\,m$. The outgoing beam axis points downward with an angle $0.02092°$ and the vertical offset of the centre of the last quadrupole of the second arc from the linac axis is $2.4\,m$.

The arcs are almost identical except that in the second arc the polarity of dipole and sextupole magnets is reversed and dipole bending angles are slightly smaller

in absolute values in order to produce the net downward beam deflection. Each arc consists of four 90° cells (fig.4), constitutes a second-order achromat and is first-order isochronous.

All arc quadrupoles (totally 18 quadrupoles in two arcs, each $0.5\,m$ long) have the same pole tip field, to permit powering them in series, and the sextupoles are powered in a three-family configuration (totally 24 sextupoles, each $0.25\,m$ long). Bending magnets are assumed to be rectangular dipoles and each arc features four $2.5\,m$ long dipoles (main dipoles) for generation of vertical dispersion and four additional weak $0.5\,m$ long dipoles for control of linear isochronicity. Because the net deflection angles of both arcs are slightly different, powering of dipoles requires four independent power supplies.

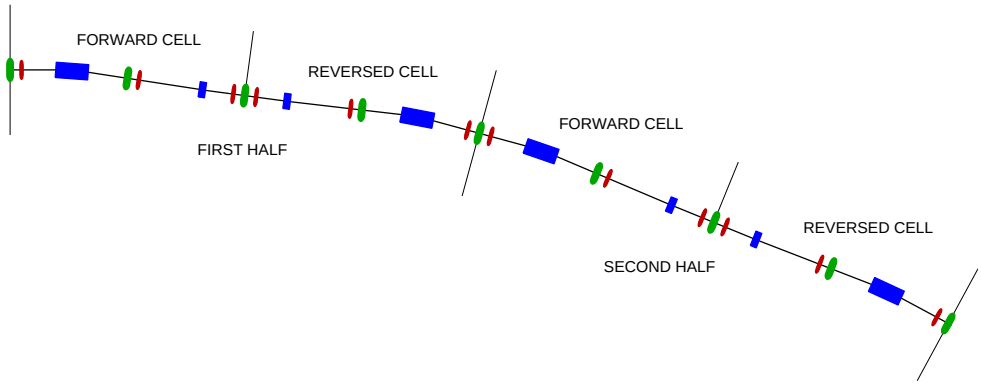

Figure 2: First arc of the XFEL post-linac collimation section and symmetries of magnet arrangement.

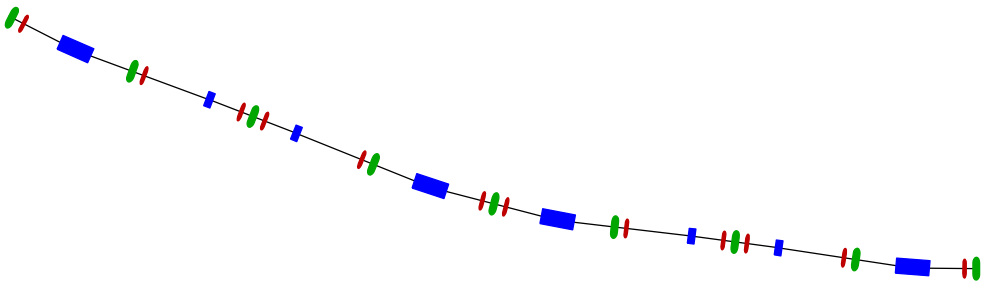

Figure 3: Second arc of the XFEL post-linac collimation section.

The first arc will collimate transverse positions of incoming particles and the second, after a shift of vertical and horizontal betatron phases by odd multiples of 90°, their transverse momenta. The energy and vertical plane collimation will be done simultaneously, and therefore the ratio of dispersion to vertical betatron function

at collimator locations has to be properly adjusted in order to achieve the required transverse and energy collimation depths. Because, according to the optics design, dispersion can not be varied during machine operations, the rough preliminary adjustment was made already during design stage by appropriate selection of the arc parameters, and the operational flexibility will be provided by usage of collimators with exchangeable apertures and by tuning betatron functions at the collimator locations.

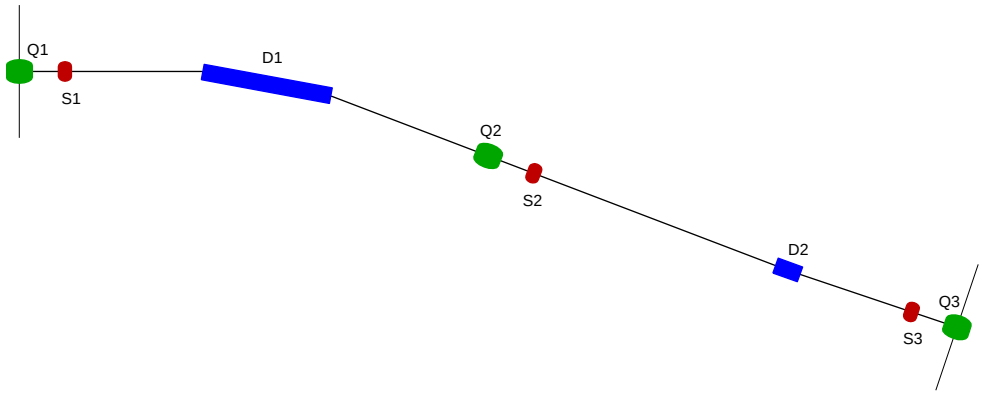

Figure 4: Forward cell of the first arc. The distance between points marked by vertical lines is $18\,m$ as measured along curved beam path.

Let us consider the first arc in more detail. The first and the second halfs of this arc are identical (see fig.2) and have a transfer matrix equal to the minus identity matrix. This means that input matching conditions are preserved in the arc centre and at the arc exit. On the other hand, betatron functions at the exit of the forward cell are inversely proportional to the betatron functions at the arc entrance. That allows us to increase them in the second half of the forward cell, where the dispersion is also large, to the values required for the protection of the collimators in the case of an aberrant beam by reducing incoming betatron functions to sufficiently small values.

The drawback of this scheme (usage of "mismatched" 90° cells) is that a relatively strong focusing field is required in the matching sections and in the phase shifter. Several approaches to solve this problem[1] were considered: usage of long quadrupoles, usage of short quadrupoles placed next to each other and usage of short quadrupoles with reduced bore radius [3]. The decision was made to use long ($2\,m$ long) quadrupoles, because the usage of short quadrupoles placed next to each

[1] According to design specifications the maximum pole tip field for all magnetic elements should not exceed $1\,T$ at $25\,GeV$ beam energy. Note also that as the minimum space between magnets we keep a distance $0.5\,m$ and that the length of a magnet means its magnetic length.

other not only requires additional length, but also makes the chromatic properties of the system worse, and because the usage of quadrupoles with reduced bore radius introduces additional limiting apertures into a system, where the most limiting apertures must be the collimators.

Totally eight $2\,m$ long quadrupoles will be used, two in the entrance and two in the exit matching sections, and four in the phase shifter. The remaining quadrupoles in the system straight sections are similar to the arc quadrupoles and are $0.5\,m$ long (see figs. 5, 6 and 7).

The quadrupoles in the phase shifter are placed symmetrically with respect to the phase shifter centre, and the same is applicable to their power supply connections. Thus 15 independent power supplies are required for powering quadrupoles in the straight sections and, in total, 23 power supplies for powering all magnets of the entire post-linac collimation system.

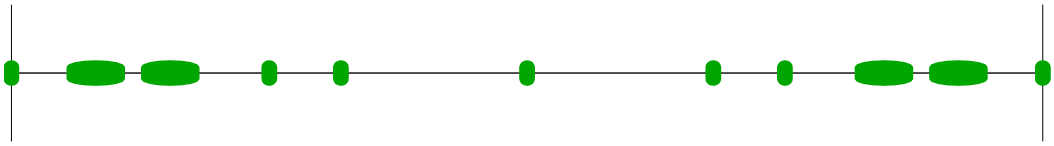

Figure 5: Phase shifter. Last quadrupole of the first arc and first quadrupole of the second arc are also shown. The distance between points marked by vertical lines is $36\,m$, which is equal to the length of two arc cells.

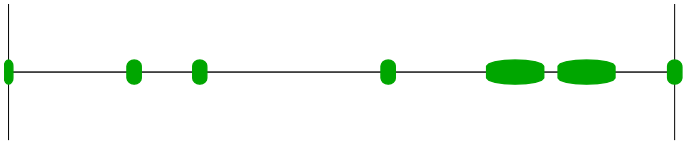

Figure 6: Entrance matching section. Last linac quadrupole and first quadrupole of the first arc are also shown. The distance between points marked by vertical lines is $23.34\,m$.

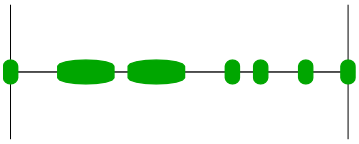

Figure 7: Exit matching section. Last quadrupole of the second arc and first quadrupole of the downstream distribution system are also shown. The distance between points marked by vertical lines is $11.97\,m$.

3 Adjustment of Linear Isochronicity

In the design described in the TDR [7] only four dipoles per arc were used and the linear momentum compaction of the whole collimation system (r_{56} matrix coefficient) was approximately equal to $-0.8\,mm$ [2], which at that time was considered as acceptable value. In later studies of the microbunching instability it was found that even such a small value can not be neglected in the calculation of the gain of this instability and that, in order to reduce this gain, it is desirable to have r_{56} of the collimation section equal to zero or, even better, to bring it to a positive value of about $0.2\,mm$ [8].

Because some other reasons for the choice of the linear momentum compaction could appear and it is not completely clear yet, what value of r_{56} is preferable, we made system modifications in such a way, that though r_{56} could not be varied dynamically during machine operations, no immediate design decision is required. In any moment, before start of the construction, linear momentum compaction can be adjusted within about $\pm 1\,mm$ limits while keeping space positions not only of the system end point and the system straight sections but also of the arc centres unchanged, as can be seen in fig.8. The design which we describe in this paper (**baseline design**) is the first-order isochronous beam line with $r_{56} = 0$.

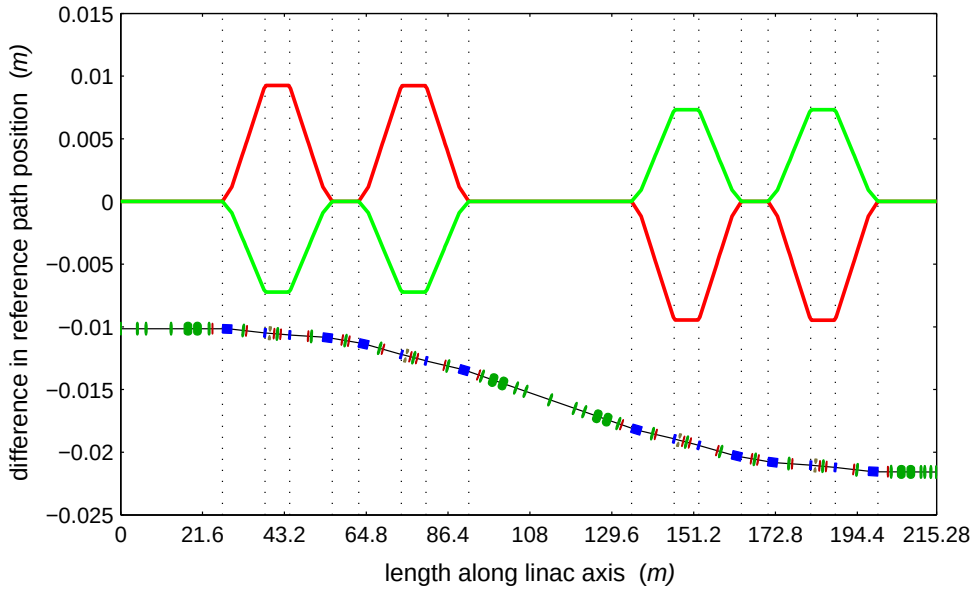

Figure 8: Changes in the vertical position of the isochronous beam line with $r_{56} = 0$, which are required to bring linear momentum compaction of the collimation section to the value $r_{56} = -1\,mm$ (red curve) and to the value $r_{56} = +1\,mm$ (green curve).

[2]The sign and, generally speaking, absolute value of r_{56} coefficient depend on the choice of variables used for description of the longitudinal beam dynamics. The exact variables, which we are using throughout this paper, can be found in Appendix A.

4 Passive Survival of Collimators

The collimators must be the most limiting apertures in the beam transport line from the accelerator to the undulators: when a bunch train comes out of the linac with a large orbit and/or energy error, the collimators should intercept the beam and should be able to withstand a direct impact of such number of bunches which can be delivered to their locations until a failure will be detected and the beam production in the RF gun is switched off.

Taking the response time of the emergency detection electronics $t_{em-detect} = 200\,ns$, the time to switch the RF gun off, $t_{gun-off} = 1000\,ns$, and the length $l_{linac} \approx 1700\,m$ for the injector and linac, an upper estimate of the number of bunches n_b which can hit the collimator is given by

$$n_b \;\leq\; \frac{1}{\Delta t_b} \cdot \left(t_{em-detect} \;+\; \frac{l_{linac} \;+\; l_{det-electr}}{10^{-9} c_s} \;+\; t_{gun-off} \;+\; \frac{l_{linac} \;+\; l_{col-loc}}{10^{-9} c} \right). \quad (1)$$

Here $\Delta t_b\,[ns]$ is the bunch spacing, $c\,[m/s]$ is the speed of light, $l_{det-electr}$ and $l_{col-loc}\,[m]$ are the distances from the linac exit to the detection electronics and to the collimator location, respectively. As the signal velocity $c_s\,[m/s]$ we will take the value $c_s = c\,/\,1.6$.

For $\Delta t_b = 200\,ns$ (minimal proposed bunch spacing, see [7]) and the length of the collimation system approximately equal to $200\,m$, a collimator has to withstand an impact of about 80-90 bunches and in the worst, but theoretically still possible, case all these bunches could hit it exactly at the same point. It means that the beam size at the collimator has to be blown up using linear optics to reduce the peak particle density to the level acceptable for the chosen collimator material.[3]

Several different materials were considered and compared in [9] as candidates for collimator manufacturing including pyrolitic graphite (carbon), beryllium and titanium. The interaction of a bunch with a collimator was investigated using the EGS4 code [10] and was followed by rough stress analysis. The simulation results, parts of which are shown in figs. 9 and 10, show that the pyrolitic graphite has, as it is well known, the best survival properties and therefore tolerates the smallest β-functions at collimator locations (25-30 m). Next comes beryllium with β-functions of about 110-120 m and titanium alloy (which performs better than pure titanium) giving tolerable β-functions of about 180-220 m.

Of these choices, we have selected titanium alloy as collimator material for the same reasons as listed, for example, in [11]: it has a higher conductivity and lower outgassing than carbon; titanium is less expensive to machine than beryllium (because beryllium flakes and dust are toxic); titanium is a far more common accelerator and engineering material and the minimal β-functions which it can tolerate are still manageable by the proposed optics design.

[3] The relatively large beam size is needed at the collimator locations not only in order to guarantee their survival during occasional beam impacts, but also in order to have the possibility to use collimators with large enough physical apertures.

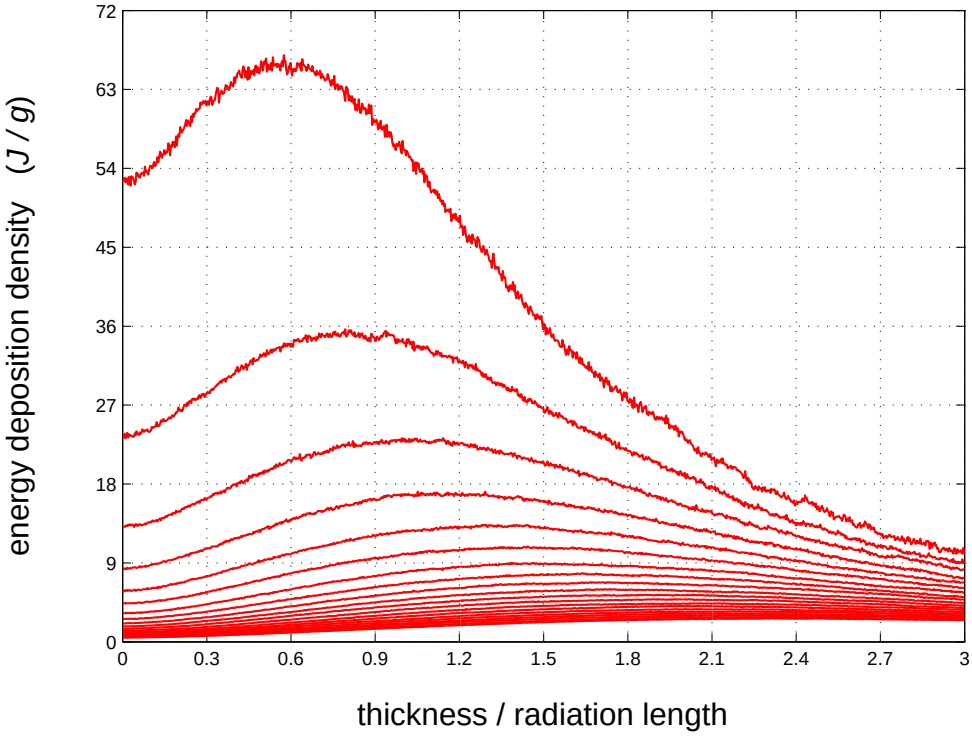

Figure 9: Energy deposition in the titanium slab from a single bunch, as a function of longitudinal position for different beam spot sizes $\sigma_x = \sigma_y = 10, 20, 30, \ldots, 210\,\mu m$ (upper to lower curves). The interaction of a gaussian bunch (bunch charge - $1\,nC$) with a slab was investigated using the EGS4 code, where a beam of 20 GeV electrons was fired into a 3 radiation length long titanium block. The thickness of the material is normalized to the radiation length $X_0 = 3.56\,cm$.

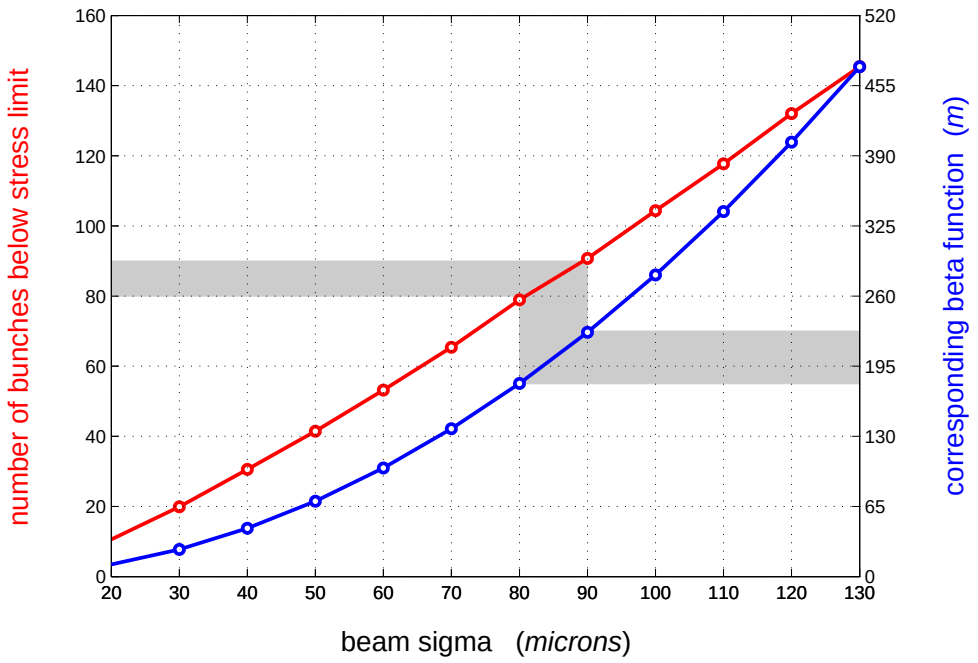

Figure 10: Maximal number of bunches (bunch charge - $1\,nC$) at which the local stress created by instantaneous temperature rise due to beam impact nowhere within a 3 radiation length long collimator made from titanium alloy exceeds the stress limit as a function of beam size $\sigma_x = \sigma_y = \sigma$ (red curve). Blue curve shows betatron function required to produce an equivalent beam size, assuming normalized emittances $\varepsilon_{nx} = \varepsilon_{ny} = 1.4\,mm \cdot mrad$ and beam energy - 20 GeV.

5 Linear Lattice Functions

According to the system design the arcs are tuned to become second-order achromats and this, together with the fixed system geometry and the requirement of the first-order isochronicity, completely determines the setting of the arc magnets and also the behaviour of the linear dispersion function.

Thus modifications of the betatron functions along the collimation section can be provided only by retuning of quadrupoles in the matching sections and in the phase shifter. This is not a limitation in our case, because the design of these sections is done in such a way that with appropriate adjustment of their quadrupoles we are not only able to provide betatron functions of about $200\,m$ at the points where the collimators are located (**standard collimation optics**), but are also able to translate smoothly the standard collimation optics into an optics with regular FODO-like transport through the entire collimation section.

This flexibility seems to be an important property of the designed system and could be extensively used during machine commissioning and/or during measurements of beam parameters. For example, commissioning could start with optics set to provide regular FODO-like transport and with sextupoles switched off and then, with experience gained, this optics can be translated step by step into the standard collimation optics.

Below in this paper we consider in more details the following four setups of the linear optics in the collimation section (operational modes):

- standard mode (A) : betatron functions of about $200\,m$ at the points where the collimators are located
- relaxed mode (B) : smaller beta functions (of about $100\,m$) at the collimator locations and, therefore, reduced sensitivity to quadrupole errors; can be used for commissioning or for operations with reduced beam power
- FODO-like transport (C) : FODO-like transport through the arcs of the collimation section, but with betatron phases still changed by odd multiples of 90° in the phase shifter; has good chromatic properties already with sextupoles switched off
- FODO-like transport (D) : FODO-like transport through the entire collimation section; in comparison with mode C, only three quadrupoles from nine in the phase shifter are switched on; has the lowest sensitivity to quadrupole errors

Betatron functions corresponding to these operational modes can be seen in figs. 11 and 12, and the linear dispersion, which is independent from setting of quadrupoles in the matching sections and in the phase shifter, is shown in fig.13. Note that in these and in all following later plots the symbol x denotes motion in the bending plane of our system, i.e., instead of the system deflecting in the vertical plane, it is more convenient for us to study the system rotated by 90° and thus deflecting in the horizontal plane.

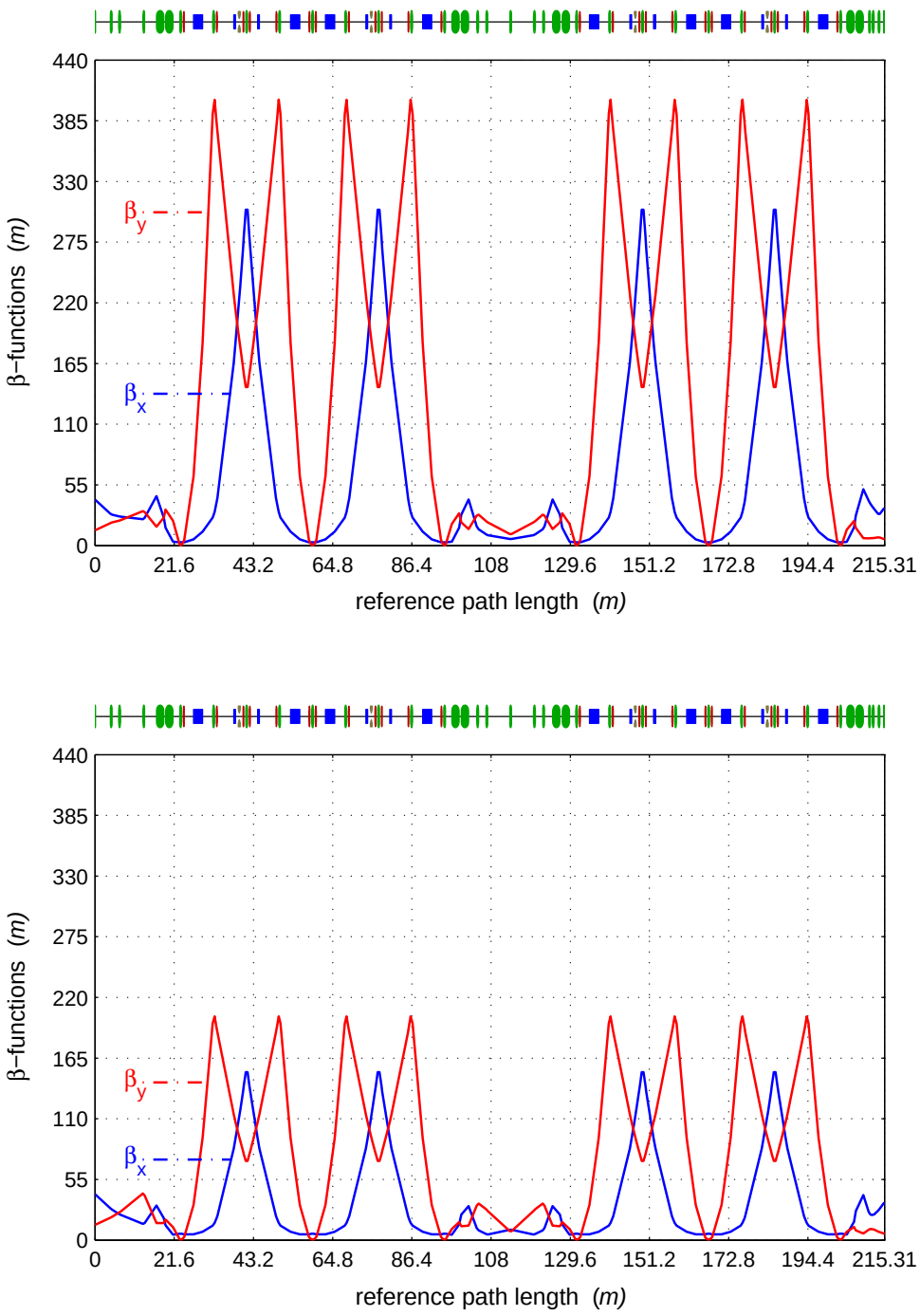

Figure 11: Betatron functions along the XFEL post-linac collimation section corresponding to operational modes A (top) and B (bottom).

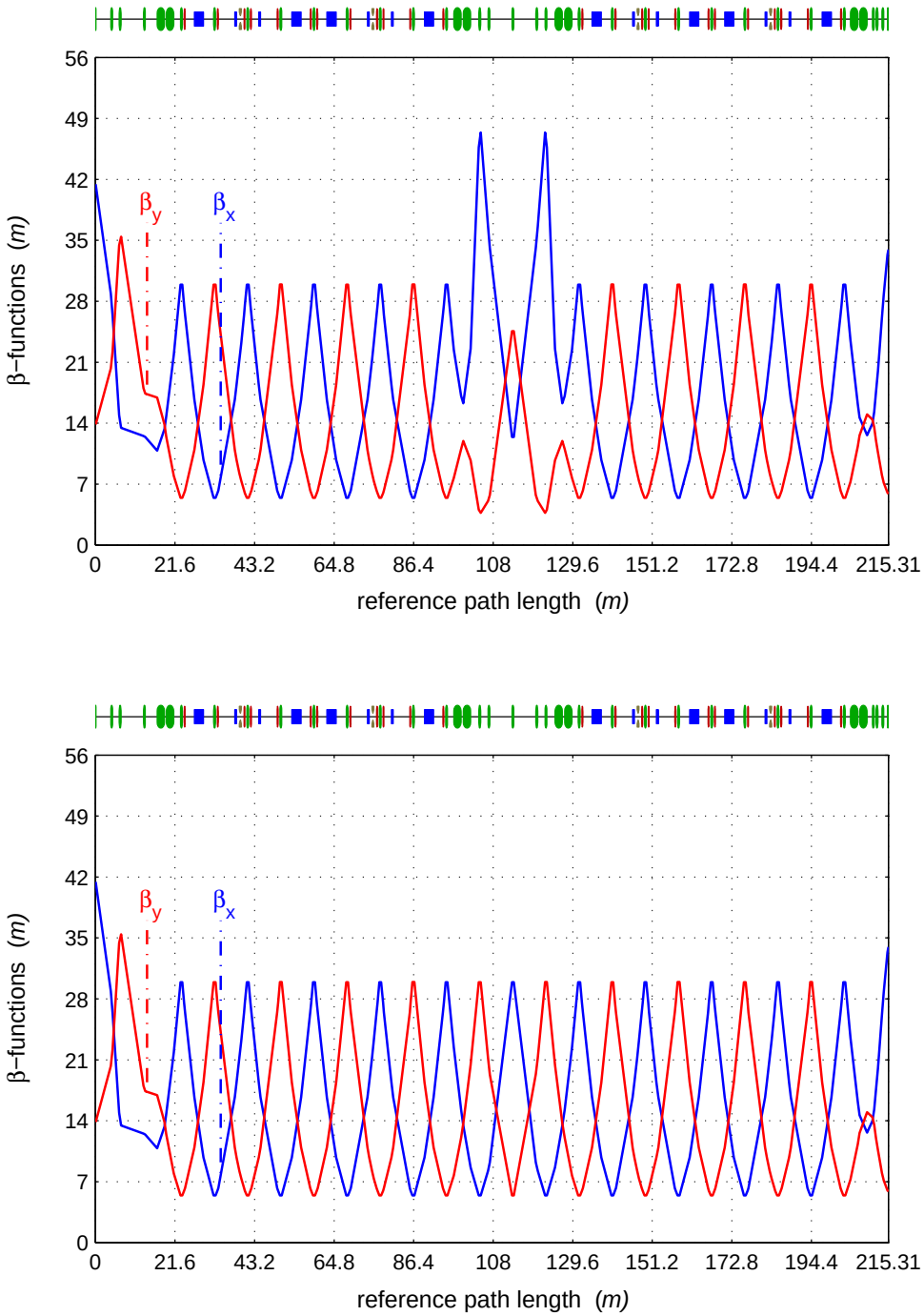

Figure 12: Betatron functions along the XFEL post-linac collimation section corresponding to operational modes C (top) and D (bottom).

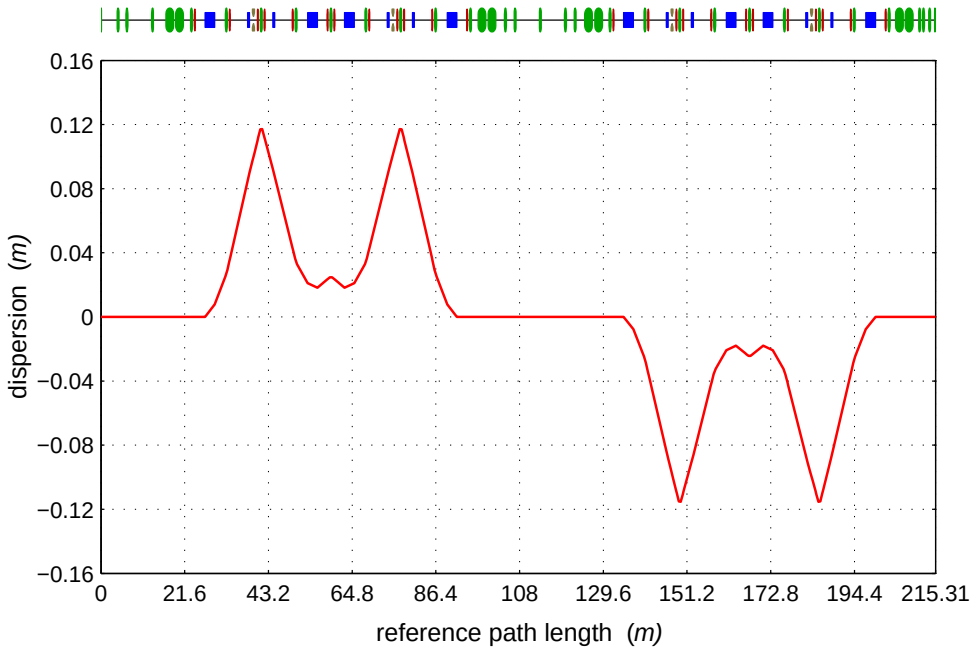

Figure 13: Dispersion function along the XFEL post-linac collimation section.

6 Details of First and Second Order Optics Design

The optics of the collimation section has to satisfy simultaneously two different and partly conflicting requirements. Large beam spot size requested at the collimator locations and, in the same time, the possibility to transport bunches with different energies (up to $\pm 1.5\%$ from nominal energy) while preserving with good accuracy energy independent input and output matching conditions[4], make the control of chromatic effects one of the main issues in the design of the optics in the collimation section. Without correction the chromatic aberrations are unacceptable as can be seen in fig.14[5] and, therefore, introduction of chromaticity correcting sextupoles becomes essential in improving overall system performance.

[4]We assume that the matching conditions at the linac exit stay fixed while the beam energy changes within $\pm 1.5\%$ limits (it does not look to be a problem to organize small energy variations in the linac while preserving output betatron parameters, because the linac focusing structure is a regular sequence of 60° FODO cells). As concerning beam transport downstream of the collimation section, the downstream system must be capable of transporting beams with energy offset to undulators and through undulators starting from initial conditions which also are energy independent and, nevertheless, retaining beam parameters required for the FEL process. Thus the collimation section, as a part of the transport line from accelerator to undulators, should be able to work as a matching section connecting (with good accuracy within $\pm 1.5\%$ limits) energy independent upstream and downstream betatron parameters.

[5]All tracking results presented in this paper are shown for the beam energy equal to $17.5\,GeV$ and normalized emittances $\varepsilon_{nx} = \varepsilon_{ny} = 1.4\,mm \cdot mrad$.

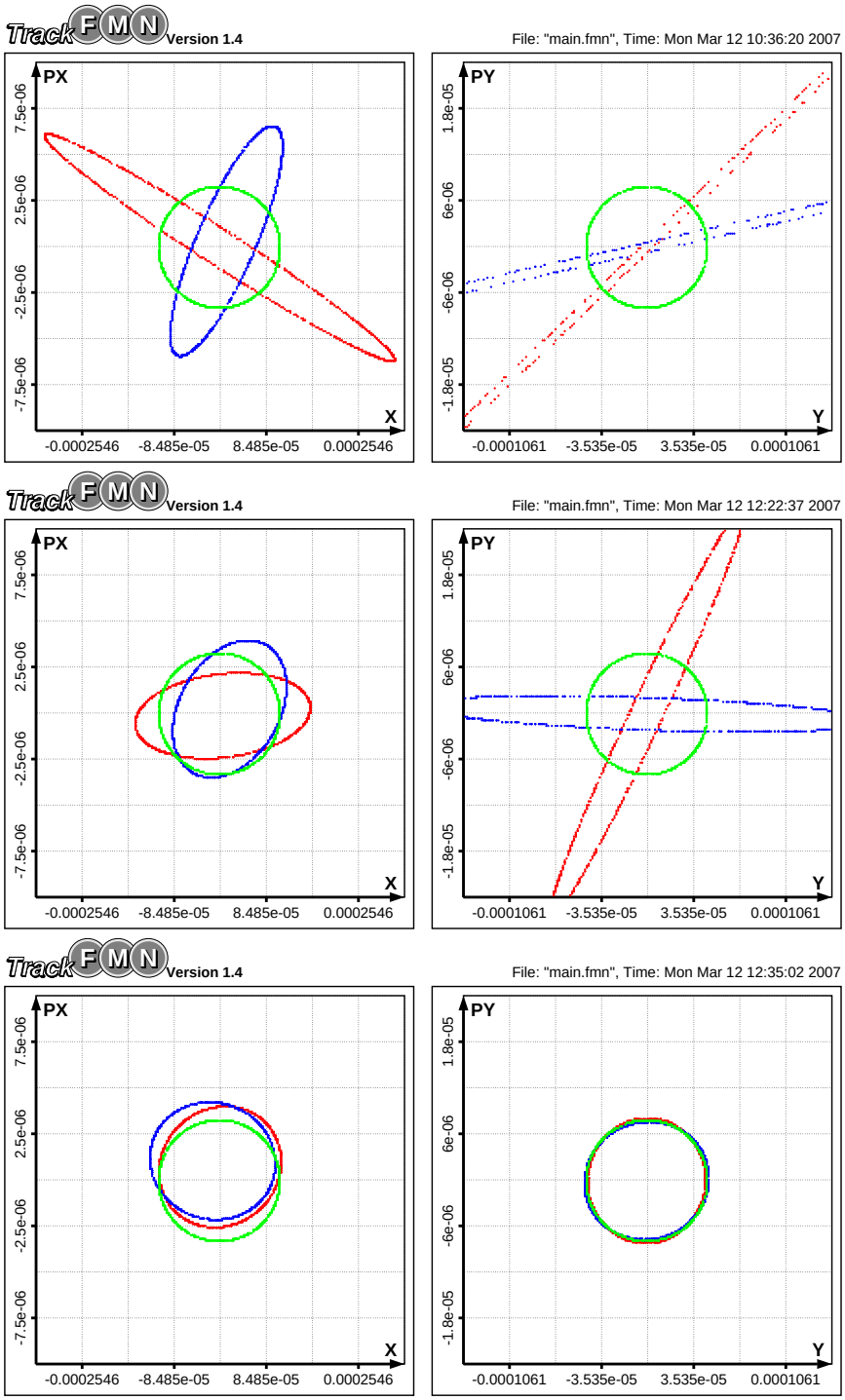

Figure 14: Phase space portraits of monochromatic $3\sigma_{x,y}$ ellipses (matched at the entrance) after tracking through the entire collimation section. The relative energy deviations are equal to -1.5%, 0% and $+1.5\%$ (red, green and blue ellipses, respectively). Optics A, B and C (from top to bottom) with sextupoles switched off.

There are different approaches to the problem of compensation of chromatic effects, and the first try was to use sextupoles at locations of nonzero dispersion for correction of chromatic aberrations in the transfer map of the entire collimation section. It was considered as unsuccessful for the following reasons. Firstly, according to the formulas (66) and (88), it is, in general, impossible to make all linear chromatic aberrations and the second order dispersions vanish simultaneously without linear position and linear angular dispersions (r_{16} and r_{26} matrix elements) equal to zero at the arc centres, which gives additional constraints for the linear optics design and, in practice, means introduction of additional quadrupoles into the arc structures. Secondly, even with linear dispersions corrected to zero at the arc centers, the sextupoles has to be retuned whenever the decision is made to change the setting of quadrupoles in the matching sections and in the phase shifter. Finally, besides all of that, in all our attempts to rearrange the linear lattice design the sextupole strengths required for reduction of chromatic aberrations to an acceptable level were too large and dynamics was spoiled not by chromatic effects but by higher order nonlinearities.

The second attempt was to use sextupoles to compensate chromatic dependence of betatron parameters on energy variations for the particular matching conditions given at the linac exit. But, as it was found, it is insufficient to correct only beta and alpha functions. The energy dependence of phase advances also has to be corrected, at least between collimator locations, because otherwise it leads to nonnegligible reduction of collimator apertures (see fig.23 in the next section). With this additional requirement the problem becomes practically equivalent to the problem of the transfer map correction and, therefore, suffers from the same difficulties.

The solution, which we found to be most adequate to the design requirements, is, in some sense, a combinations of the two above approaches. We compensate the arc chromatic effects in the maps by tuning arcs to become second-order achromats. Reduction of chromatic aberrations in the system straight sections is done for the particular betatron functions transported through these parts and without involving sextupole fields, simply by an accurate drift-quadrupole optics design. Let us discuss this solution in more detail.

There are two symmetries of the arrangement of the arc dipole and quadrupole magnets, which can be seen in fig.2 and which can be used in order to make the arc an achromat. The first is the four-cell symmetry of the type FRFR, where the forward cell (F) is followed by reversed cell (R) and then this two-cell configuration is repeated once more. The second symmetry is to consider the arc simply as an repetition of two identical cells (FF symmetry). The symmetry FF requires 6 independent sextupole families to be used in order to achieve a second order achromat while with the symmetry FRFR only 4 independent sextupole families are needed (consult Appendices B and C for theoretical details). But because one has to put sextupoles into the arc in such a way that the symmetry is preserved, the minimum number of sextupoles required for one arc is 16 for the symmetry FRFR and only 12 for the

symmetry FF.

The first decision made was to set arc quadrupoles according to the symmetry FRFR because with conditions (50) fulfilled[6] the first order requirements of the symmetry FF will be satisfied too, and then make an accurate search for an optimal sextupole configuration. With a specially written program it was found that for the best solutions the integrated sextupole field is about the same for both symmetries and that, more important, the maximal value of the sextupole strengths in these solutions is also about the same. This makes the usage of FF symmetry definitely preferable, because less sextupoles are required. The second optimization step was the attempt to reduce the integrated sextupole field, maximal sextupole strength and number of independent sextupole families while keeping chromatic aberrations to an acceptable level. The good practical solution uses 12 sextupoles per arc; the sextupoles are introduced into the arcs according to the symmetry FRFR and are powered in a three-family configuration (all 24 sextupoles of both arcs) following the same symmetry; the integrated sextupole field is reduced by 25% and the maximal sextupole strength is smaller by 30% as compared to the best solutions given for the theoretically perfect second-order achromats.

As concerning design of the system straight sections (figs. 5, 6 and 7), it is known that though a straight drift-quadrupole system can not be made an achromat (see, for example, [12, 13, 14]), it can be made a second-order apochromat with respect to certain incoming beam ellipses, i.e. it can transport these beam ellipses (envelope functions) without introducing first-order chromatic distortions.[7] In practice, we did not try to make straight sections to become theoretically perfect second-order apochromats. The problem was considered as a matching problem with additional constraints, which were the reductions of apochromatic aberrations to an acceptably small level. With the help of a specially written program the number of quadrupoles in the phase shifter and in the entrance and exit matching sections, and the distances between these quadrupoles were carefully selected in order to be able to cover all expected ranges of the betatron parameters while preserving good chromatic properties of the beam transport. Note that because the phase shifter has to provide a shift of vertical and horizontal betatron phases by odd multiples of 90° and because its entrance and exit beta functions are equal to each other for all operational modes with alpha functions always equal to zero, we arranged its quadrupoles mirror symmetric and thus have reduced the number of independent apochromatic aberrations from four to two.

The price paid for the usage of (interleaved) sextupoles to correct chromatic aber-

[6]Four independent parameters are required in order to satisfy conditions (50) and to make diagonal elements of the forward cell matrix equal to zero. One may choose as such parameters three quadrupole gradients plus, for example, shift of the Q2 quadrupole (see fig. 4) away from the cell center. Because focusing asymmetry introduced by dipole magnets is very weak, the good practical solution can be obtained using absolute value of quadrupole gradients as a single fitting parameter. This permit to power all quadrupoles of both arcs using only one power supply.

[7]Following [15] we have found convenient to use the term *apochromat* for such type of focusing.

rations is, as usual, some increase of the effect of high-order nonlinearities (see fig.15), which does not look to be a serious problem. Note that the tracking result shown in the bottom of fig.15 was obtained with both, x and y, offsets being simultaneously nonzero at the system entrance. One may compare this with the tracking result shown in fig.16, where, at the system entrance, particles had only horizontal or only vertical offset from the beam axis. The effect of energy offsets, optics nonlinearities and transverse beam offsets at the system entrance on the evolution of the beam spot size along the collimation section can be seen in fig.17

The resulting performance of the entire post-linac collimation section with respect to the beam energy change fulfills the design specification and can be seen in figs. 18 and 19.

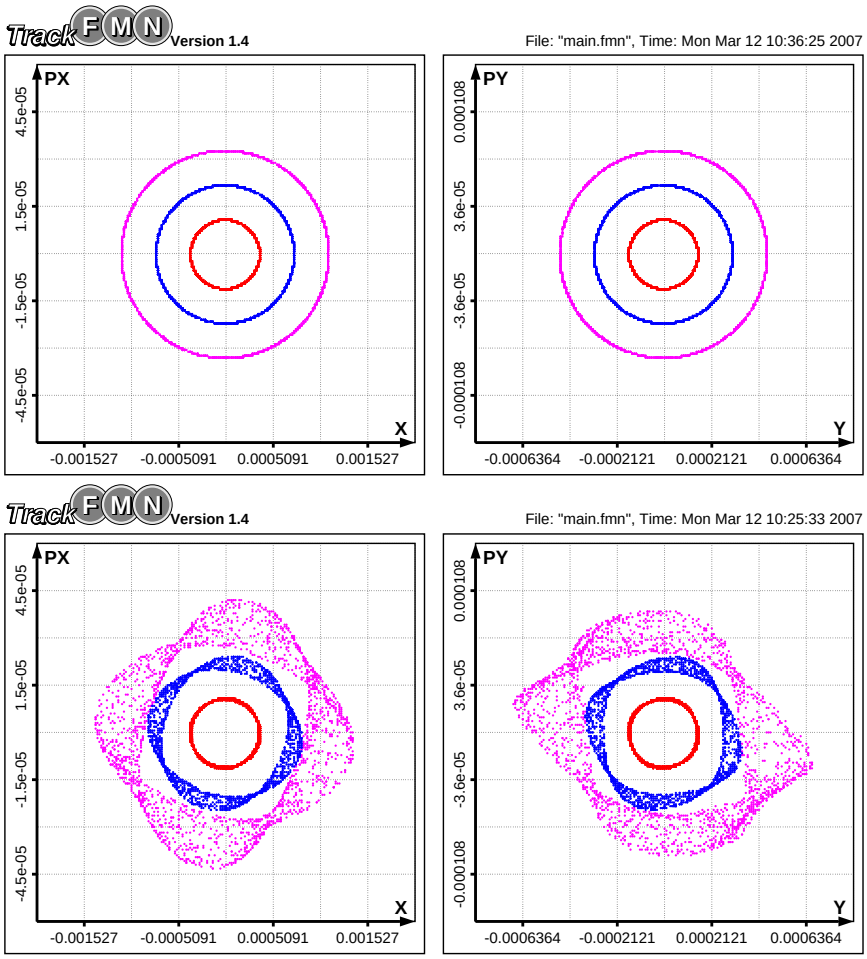

Figure 15: Results of particle tracking with nominal energy through the entire collimation section. At the entrance these particles were uniformly distributed on the three 4-dimensional surfaces which in projections on horizontal and vertical planes form matched $10\sigma_{x,y}$, $20\sigma_{x,y}$ and $30\sigma_{x,y}$ ellipses (red, blue and magenta colors, respectively). Optics A with sextupoles switched off (top) and on (bottom).

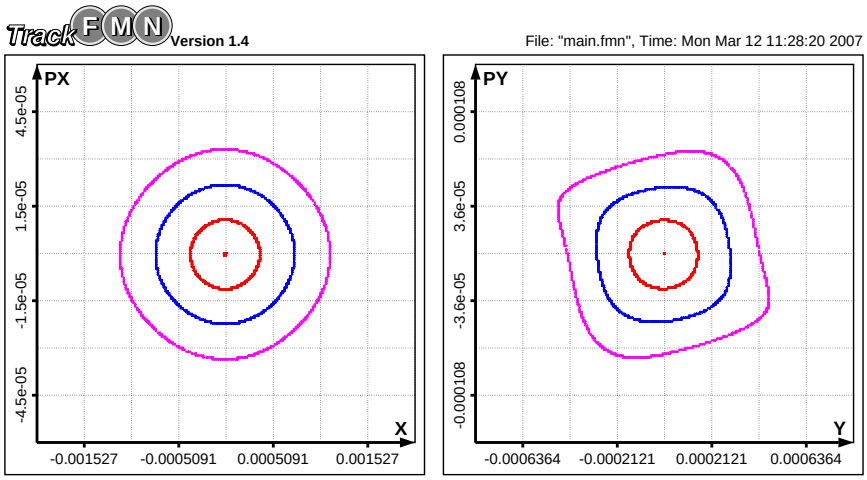

Figure 16: Results of particle tracking with nominal energy through the entire collimation section. At the entrance these particles were uniformly distributed on the perimeters of the six matched two-dimensional ellipses. $10\sigma_x$, $20\sigma_x$ and $30\sigma_x$ ellipses with y, p_y coordinates equal to zero, and $10\sigma_y$, $20\sigma_y$ and $30\sigma_y$ ellipses with x, p_x coordinates equal to zero. Optics A with sextupoles switched on.

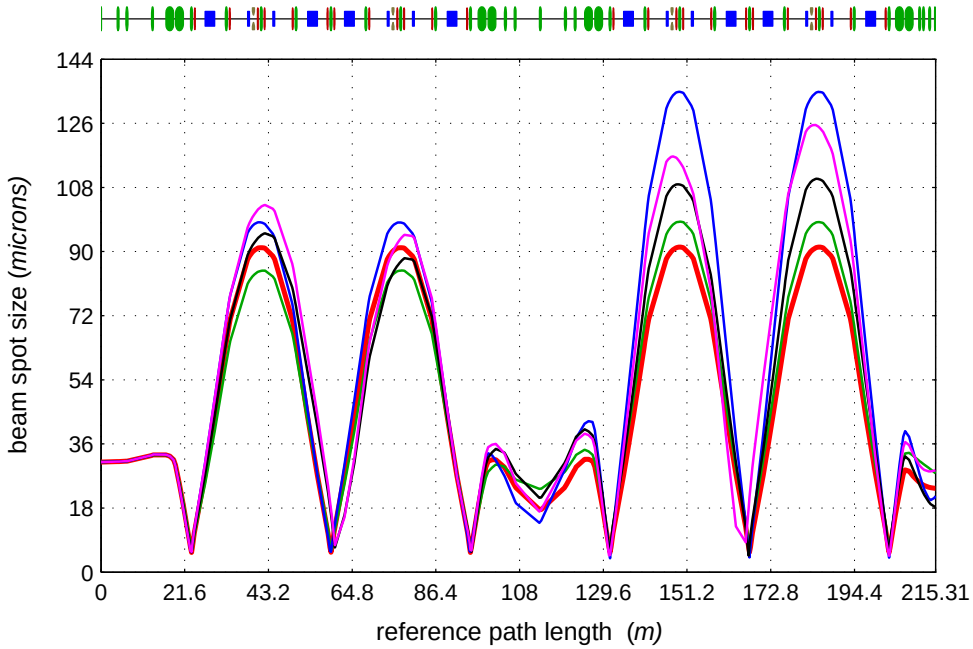

Figure 17: Evolution of beam spot size ($\sqrt{\sigma_x \sigma_y}$) along the collimation section. Red curve shows the design spot size (linear theory). All other curves are results extracted from the tracking simulations. A matched Gaussian beam at the entrance with -3% (blue) and $+3\%$ (green) energy offsets, with $40\sigma_x$-offset (black), and with both -3% energy and $40\sigma_x$-offsets (magenta). Optics A with sextupoles switched on.

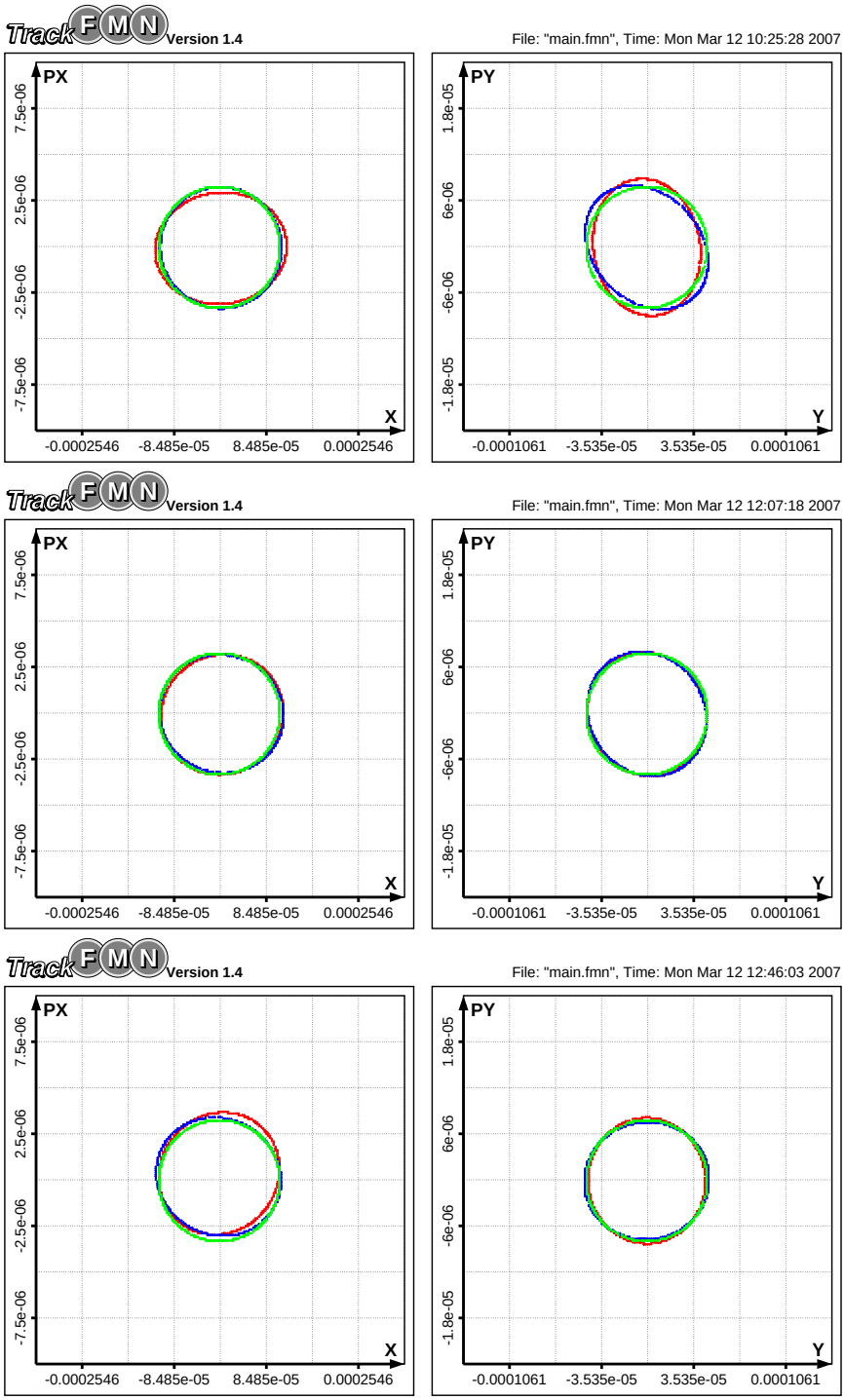

Figure 18: Phase space portraits of monochromatic $3\sigma_{x,y}$ ellipses (matched at the entrance) after tracking through the entire collimation section. The relative energy deviations are equal to -1.5%, 0% and $+1.5\%$ (red, green and blue ellipses, respectively). Optics A, B and C (from top to bottom) with sextupoles switched on.

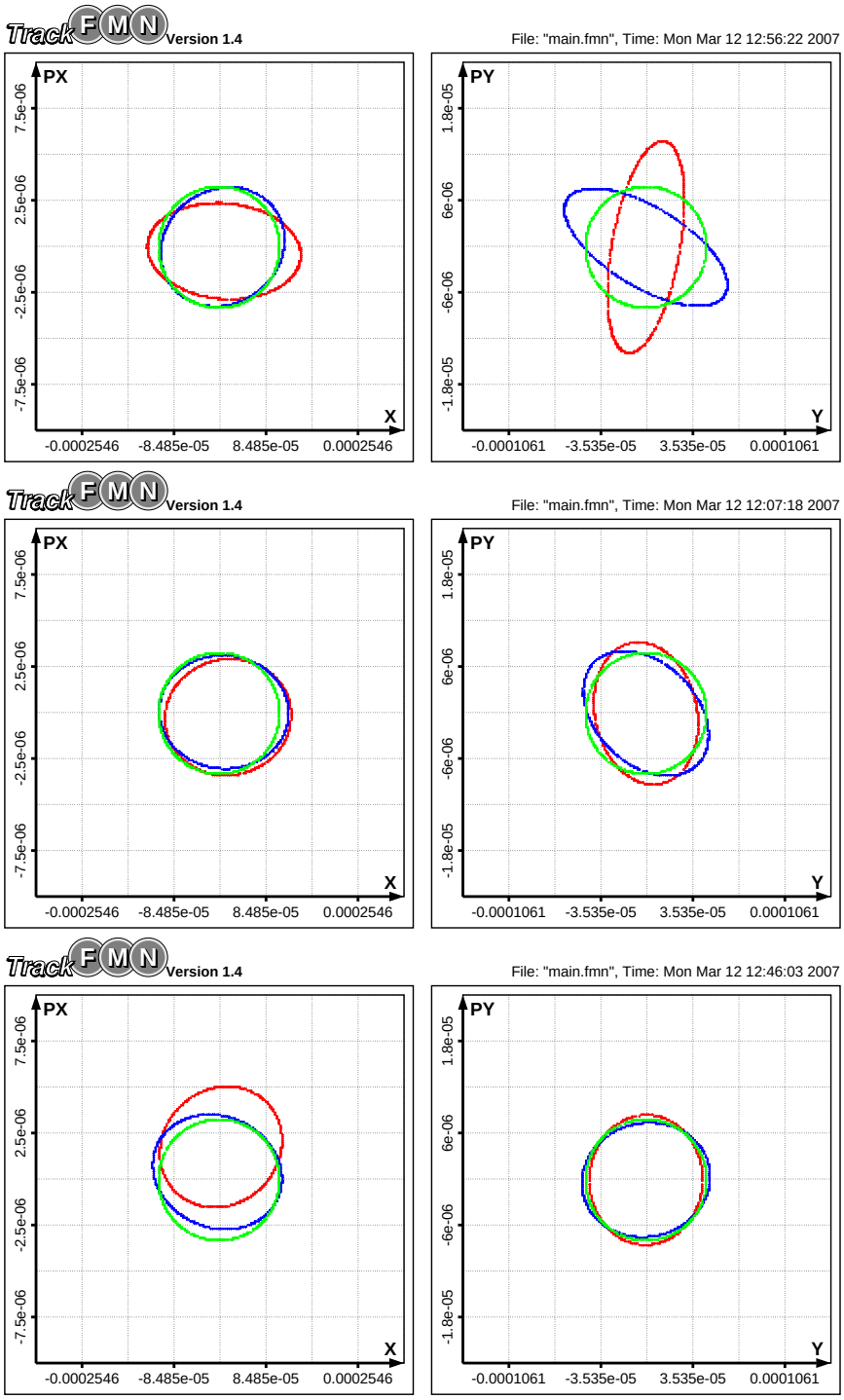

Figure 19: Phase space portraits of monochromatic $3\sigma_{x,y}$ ellipses (matched at the entrance) after tracking through the entire collimation section. The relative energy deviations are equal to -3.0%, 0% and $+3.0\%$ (red, green and blue ellipses, respectively). Optics A, B and C (from top to bottom) with sextupoles switched on.

7 Estimate of Required Collimator Apertures

The goal of the post-linac collimation system is to confine at its exit all particles which passed the collimation section freely (without touching collimator apertures) into such volume in phase space (**downstream dynamic aperture**), that can be safely transported through all downstream beamlines including undulator modules to the beam dumps, and to keep the number of secondary and rescattered particles which appear outside of the downstream dynamic aperture to an acceptably small level. Besides that it is desirable to avoid uncontrolled impacts of the particles coming from the linac (**primary particles**) onto the beam pipe in the collimation section, which can lead to beam pipe damage if the whole beam is off-energy and/or mis-steered.

Three different types of collimators are foreseen to be used in the XFEL post-linac collimation system to accomplish these tasks: main primary collimators, supplementing primary collimators and secondary collimators (absorbers). The principal purpose of the main primary collimators is to intercept trajectories of all primary particles which would otherwise appear outside of the downstream dynamic aperture. The main collimators will also shade a part of the beam pipe in the collimation section (but not all) from uncontrolled beam impacts. Supplementing primary collimators assist to accomplish this work or, at least, reduce the probability of such events. In the same time the supplementing collimators should not affect the transverse and energy collimation depths set by the main collimators. To improve the overall cleaning efficiency at the exit and better localize losses inside of the collimation section several absorbers placed in the shadow of the primary collimators will be used.

It is not the intention of this paper to make a systematic search for a good combination of all three types of collimators, all the more that not all input data needed for such optimization are still available (for example, not all details of the hardware design which will define the exact inner shape of the downstream vacuum chamber at current stage of the project are finalized yet). Instead we concentrate on the study of the main primary collimators whose number and locations can be chosen more or less independently from locations of other collimator types and from fine details of the hardware design.

The current proposal is that four main collimators made from titanium alloy will be used, two in each arcs (see figs. 20 and 21). Similar to the collimators which are currently in use at the FLASH facility[8] they will have round inner apertures and the possibility to interchange between three different aperture radii by an appropriate mechanics. Exchangeable apertures combined with the possibility of tuning betatron functions at the collimator locations will allow to regulate transverse and energy collimation depths separately (within some limits), despite the fact that collimators are

[8]Optics design of the FLASH post-linac collimation section can be found in [16] and some details of the mechanical collimator design are presented in [7].

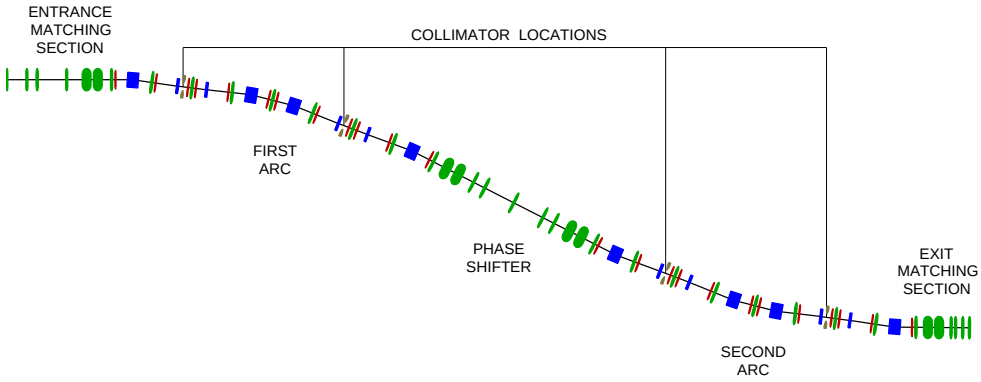

Figure 20: Locations of the main primary collimators in the XFEL post-linac collimation section.

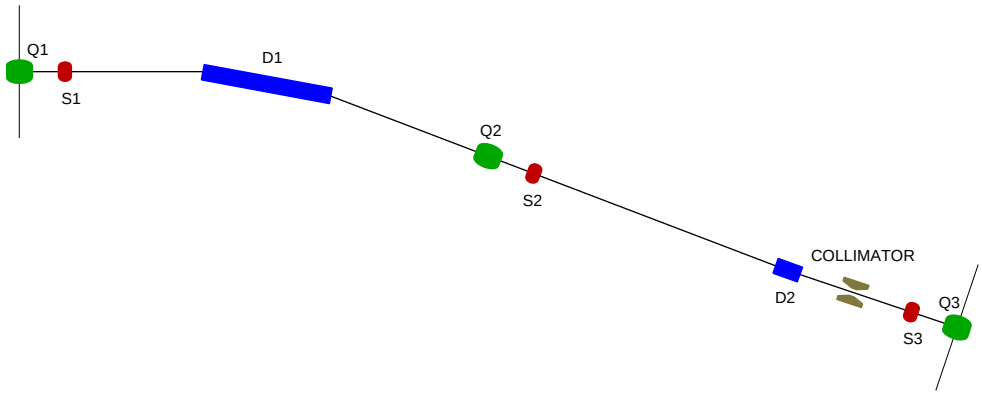

Figure 21: Location of the main primary collimator in the forward cell of the first arc.

placed in the dispersive region of the beamline. This gives an additional operational flexibility to the post-linac collimation system.

The main purpose of the studies presented below is not to define the set of apertures for each collimator already as the final recommendation for the manufacturing. Instead we show that these four collimators are capable of providing such phase space limitations at the exit of the collimation section which are sufficient for the protection of the undulator modules and other downstream equipment against off-momentum and large amplitude halo particles and also against miss-steered and off-energy beams. Note that during our investigations we have used software and algorithms developed for the study of the collimator system of the FLASH facility [16].

In order to avoid possible misinterpretation of the calculation results, let us first define accurately all components which were actually used for the estimation of the effect of the collimators on the particle phase space at the exit of the collimation section.

Distribution of incoming particles. The distribution of the particles coming into the collimation section was modeled by a set of monochromatic 4-dimensional 170-σ distributions[9] each filled with $5 \cdot 10^5$ particles. This distribution, in the projection on the real space, does not cover all vacuum chamber aperture at the collimation section entrance, but is sufficient for the study of the effect of the collimators on the particle phase space at the collimation section exit (but is, in general, insufficient for the study of the protection of the beam pipe inside collimation section), as was shown by special additional investigations. The main reason to do such additional investigations instead of simple usage of larger number of sigmas, was the desire to have a large enough number of particles per unit volume while keeping the total number of particles in reasonable limits.[10]

Particle tracking algorithm. As particle tracking algorithm the symplectic numerical integration of the Hamiltonian equations of motion in the SCOFF[11] approximation was used. Thus geometrical and chromatic aberrations were taken into account, but possible effects of extended fringing fields were not included and will be estimated later on, when we will have more or less realistic fringing field profiles (below we will see how strongly the sextupole magnets affect the size of the collimator apertures required for the undulator protection, and, because extended fringing fields introduce additional nonlinearities into the system, they also could be of some importance for the motion of particles which will have large transverse offsets at the collimation system entrance). Note that the beam dynamics code which we used for tracking is capable of simulating extended fringing fields of multipole magnets [17].

Model of collimators. In the studies presented in this paper we have used the "black absorber" model for the collimators - any particle touching them is considered as lost. All four collimators were assumed to be identical with the length equal to $20\,cm$[12] and with a circular hole as the shape of the inner collimating tube.

Criteria for undulator to be protected. At the current stage we do not track the particles which safely passed the collimation section further through all downstream beamlines, but instead check them at the exit of the collimation system and

[9] As 4-dimensional n-σ distribution we understand the distribution in which (x, p_x) and (y, p_y) particle coordinates are generated independently so as to populate uniformly the interior of n-σ_x and n-σ_y matched ellipses, respectively.

[10] With fixed number of particles per unit volume the total number of particles in the n-σ distribution is proportional to n^4.

[11] SCOFF stands for Sharp Cut-Off Fringing Field.

[12] When the collimators are considered as black absorbers, the dependence of the calculated apertures on the collimator length is relatively weak (for related discussions see [16]).

if even one lies outside of the matched ellipses

$$\begin{cases} \gamma_x x^2 + 2\alpha_x x p_x + \beta_x p_x^2 = J_x \\ \gamma_y y^2 + 2\alpha_y y p_y + \beta_y p_y^2 = J_y \end{cases} \tag{2}$$

then a protection failure is recorded.

The constants J_x and J_y in (2) are connected with the undulator parameters according to the formulas

$$J_x = \frac{r_{und}^2}{2\beta_{x,max}}, \qquad J_y = \frac{r_{und}^2}{2\beta_{y,max}}, \tag{3}$$

where r_{und} is the radius of the undulator vacuum chamber[13], and $\beta_{x,max}$ and $\beta_{y,max}$ are the maximum values of the betatron functions along the undulator.

In the following we will assume that $\beta_{x,max} = \beta_{y,max} = 30\,m$ and, instead of introducing the safety factor into (3) explicitly, will consider several different values for the radius $r_{und} = 5$, 4, 3 and $2\,mm$.

For the tracking calculations we use the beam energy equal to $17.5\,GeV$ and normalized emittances, ε_{nx} and ε_{ny}, equal to $1.4\,mm \cdot mrad$. For these beam parameters the radii $r_{und} = 5$, 4, 3 and $2\,mm$ correspond to approximately 100, 80, 60 and 40 beam sigmas (simultaneously for both planes, x and y) at the exit of the collimation system, respectively.

Calculation procedure. When the value of r_{und} in (3) and, therefore, in (2) is fixed, it is possible to begin the search of the maximum allowed aperture of the collimators (aperture which separates apertures which can protect the undulator vacuum chamber from those which can not). This search was performed using the method of bisection and separately for each monochromatic portion of the incoming 170-σ particle distribution, so that the results can be presented as a function of the energy deviation.

In part of the calculations we have used an additional requirement to avoid losses of the primary particles on the beam pipe downstream of the first collimator. In these calculations the beam pipe radius was set to the value $25\,mm$, and in all other calculations the effect of the beam pipe on the particle dynamics between collimators was not taken into account.

Some curves, obtained for the case when sextupole magnets are switched on, change their shape quite rapidly in certain regions of the energy offsets (see, for example, region between -8% and -4% relative energy deviations in fig.24). No determination was made as to whether these effects are due to actual (chromatic and geometrical) nonlinearities of the system or due to the fact that the number of

[13]The actual undulator vacuum chamber will have elliptical cross-section with the most limiting apertures being the radiation absorbers [7]. So as r_{und} we, in fact, will understand throughout this paper the radius of the cylinder which could be inscribed inside the undulator vacuum chamber.

particles per unit volume in the incoming distribution is still not large enough (or due to combination of both). Instead of that, after completion of the calculations, we set the collimator apertures to the value which is slightly smaller than the minimum obtained within the considered region of the energy offsets, and check that this value of the aperture radius is capable of providing undulator protection by tracking again through the system a set of monochromatic 170-σ distributions, but populated now with $5 \cdot 10^6$ particles.

The first figure presenting the calculation results shows the aperture radius required to block the corresponding off-energy fraction of incoming particles in the collimation section (red curve in fig.22). Because collimator pairs within each arc are separated by a minus identity transformation in the betatron space and all collimators have identical apertures, the linear theory predicts that for small energy deviations this curve should follow the line $a \cdot \mid \varepsilon \mid$, where

$$a \;=\; \frac{1}{2} \cdot \max\left(\mid D_1 \,+\, D_2 \mid, \mid D_3 \,+\, D_4 \mid\right) \;\approx\; 10\, cm\,,$$

D_n is the value of the linear dispersion at the n-th collimator location and ε is the relative energy deviation. It is indeed the case (see blue curve at the same figure) and, therefore, one has to set the aperture radii approximately to the value $N\, mm$ in order to be able to stop in the collimation section all particles with the energy offsets outside of the $\pm\, N\%$ region.

The positive effect of sextupoles on the increase of the collimator apertures required for protection of the undulator vacuum chamber can be seen in fig.23. Let us look more closely at the magenta curve in this figure, i.e. at the case when sextupoles are switched off. Though, for the nominal energy, the calculated aperture coincides with good precision with the prediction of the linear theory, it drops down almost twice due to strong dependence of betatron parameters on energy variations when the energy offset becomes nonzero. The sextupoles remove part of this chromatic dependence and thus allow to use collimators with larger radii for the protection of the undulator vacuum chamber.[14]

Figs. 24 and 25 show aperture radii calculated for two different optics (optics A and optics B, respectively). Because in the optics A the betatron functions at the collimator locations are exactly two times larger than in the optics B, the expectation from the linear theory is that the ratio of minimums of curves from these two figures corresponding to the same value of r_{und} should be equal to $\sqrt{2}$ (≈ 1.41). The real drop of apertures is smaller and changes from 1.14 to 1.26 when r_{und} decreases from 5 to $2\, mm$, which reflects the nonlinear properties of the collimation section.

[14]It does not seem that nonlinear transfer properties of the collimation system require any essential improvements. Nevertheless, it will be interesting to see in the later studies if the usage of octupoles can bring collimator apertures close to the estimation following from the linear theory than in the case when only sextupoles are used.

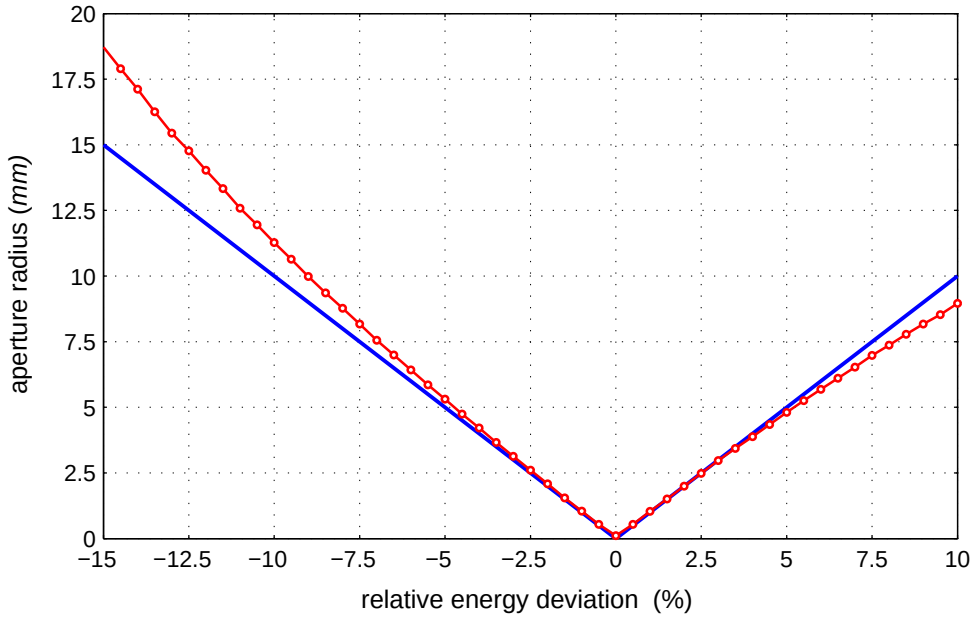

Figure 22: Red curve: aperture radius required to block the corresponding off-energy fraction of incoming particles in the collimation section. Blue curve: analytical estimate for this radius made using linear dispersion at the collimator locations. Optics A with sextupoles switched on.

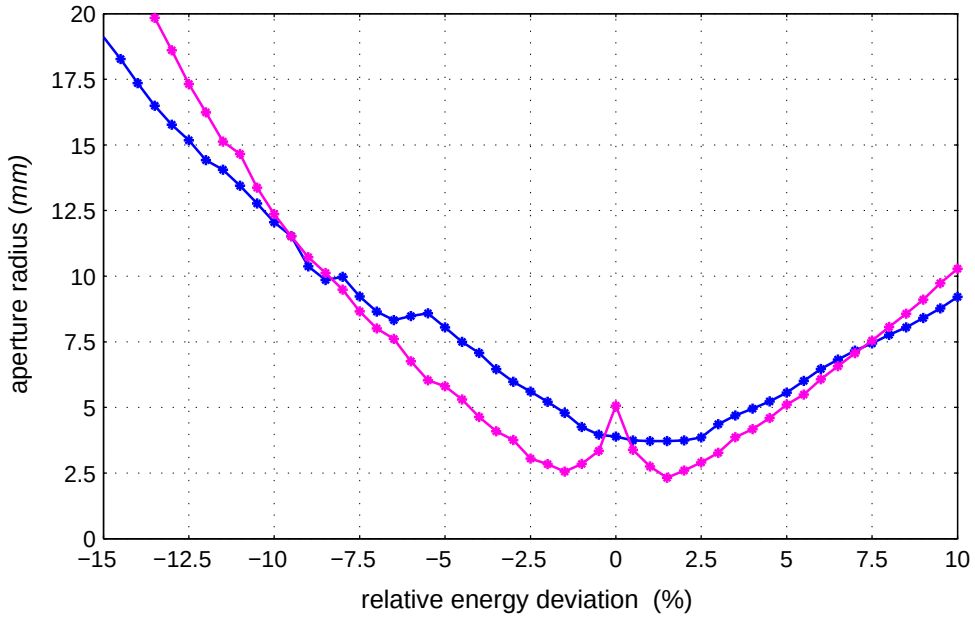

Figure 23: Aperture radius required to protect the undulator vacuum chamber ($r_{und} = 4\,mm$) as a function of the energy deviation. Optics A with sextupoles switched off (magenta curve) and on (blue curve).

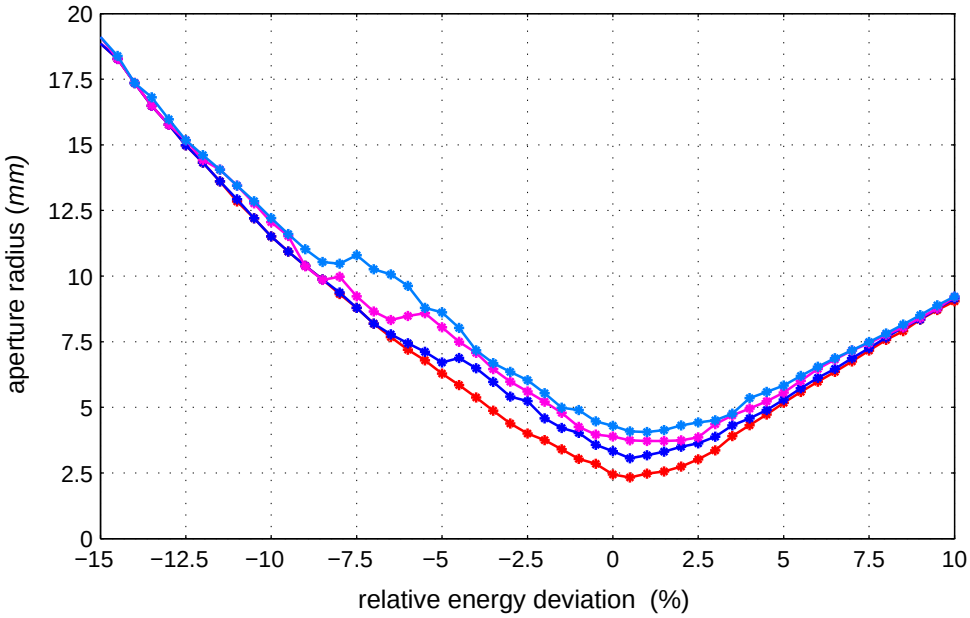

Figure 24: Aperture radius required to protect the undulator vacuum chamber as a function of the energy deviation for different values of the radius of the undulator vacuum chamber $r_{und} = 5, 4, 3, 2\, mm$ (upper to lower curves). Optics A with sextupoles switched on.

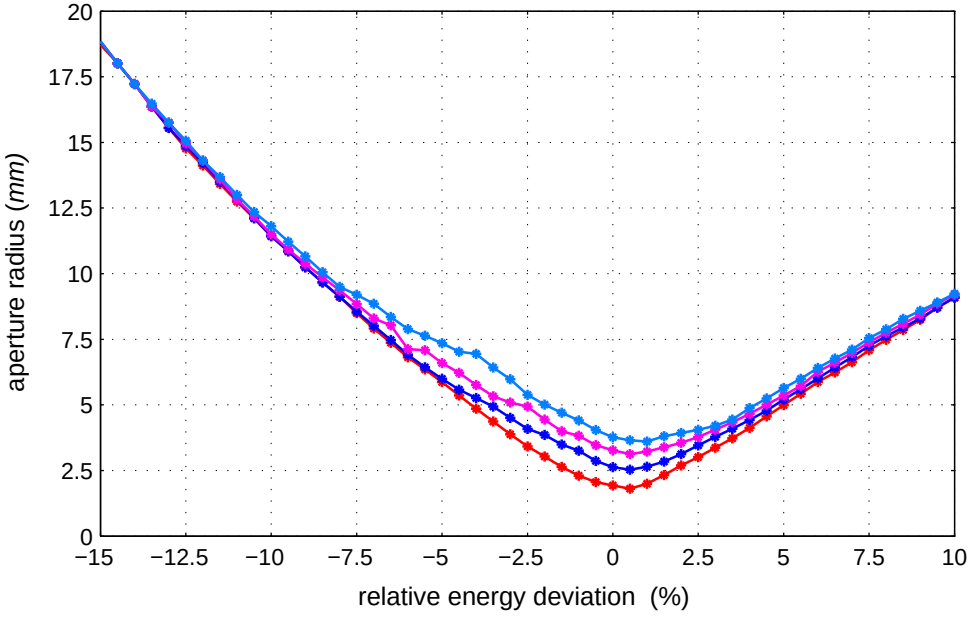

Figure 25: Aperture radius required to protect the undulator vacuum chamber as a function of the energy deviation for different values of the radius of the undulator vacuum chamber $r_{und} = 5, 4, 3, 2\, mm$ (upper to lower curves). Optics B with sextupoles switched on.

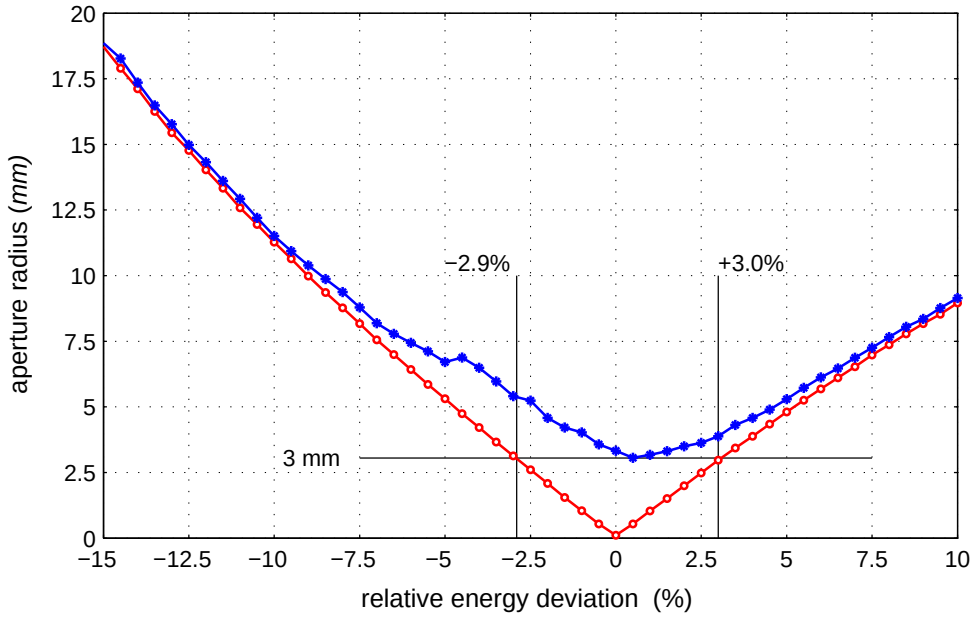

Figure 26: Blue curve: aperture radius required to protect the undulator vacuum chamber ($r_{und} = 3\,mm$) as a function of the energy deviation. Red curve: aperture radius required to block the corresponding off-energy fraction of incoming particles in the collimation section. Optics A with sextupoles switched on.

Let us set the collimator radii to the value $r_{col} = 3\,mm$, which is required to protect the undulator vacuum chamber with $r_{und} = 3\,mm$ (equality $r_{col} = r_{und}$ is accidental), and look in more details on the phase space limitations at the exit of the collimation system provided by these collimator apertures. When collimators are considered as the black absorbers, all particles with the relative energy deviation smaller than about -2.9% or larger than about $+3.0\%$ will be stopped in the collimation section completely, as can be concluded from the plot shown in fig.26. In the transverse phase space, no of particles should appear outside of the region bounded by $\approx 60\sigma_x$ and $\approx 60\sigma_y$ ellipses, because they are, in fact, the target ellipses set at the exit of the collimation system corresponding to the choice $r_{und} = 3\,mm$ for the undulator vacuum chamber. But, in the presence of dispersion at the collimator locations, the collimators will no longer cut the transverse phase space for all values of energy offset to the same degree, and, in the presence of sextupoles, this cut could be different for two transverse planes even for the nominal energy, as one can see in fig.27. The characterization of the transverse phase space obtained with the help of tracking simulations is presented in figs. 28 and 29. Note that curves in fig.29 show substantial difference between two collimation depths for the non-bending plane motion around nominal beam energy: calculated numerically and predicted by the linear theory. This is an important fact and it is better to consider these results as preliminary and to check them once more using larger number of particles or/and different calculation algorithm.

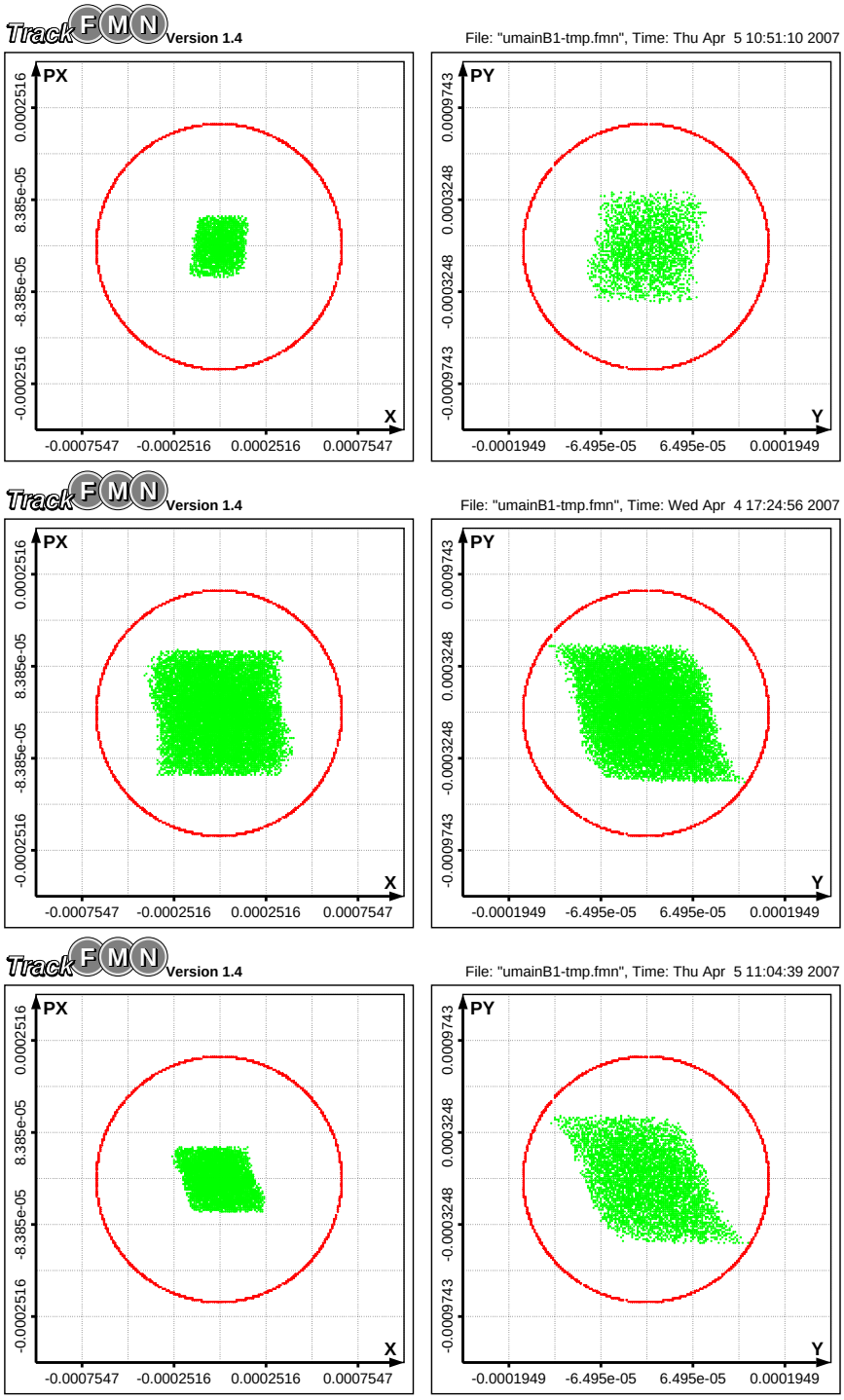

Figure 27: Results of the tracking of monochromatic 170-σ particle distributions through the entire collimation section. The relative energy deviations are equal to -1.5%, 0% and $+1.5\%$ (from top to bottom). The main primary collimators have aperture radii $3\,mm$. The target ellipses (red curves, $\approx 60\sigma_x$ and $\approx 60\sigma_y$ ellipses) correspond to $r_{und} = 3\,mm$. Optics A with sextupoles switched on.

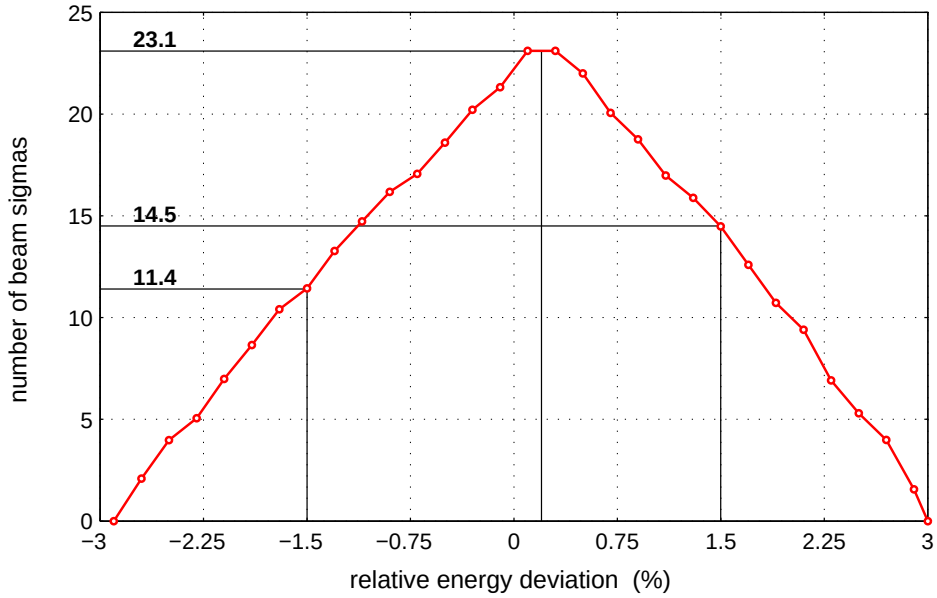

Figure 28: Number of sigmas (n) which separates corresponding monochromatic m-σ distributions into two classes: all m-σ distributions with $m < n$ will pass the collimation section freely, but among particles from any m-σ distribution with $m > n$ there exists at least one particle whose trajectory will be intercepted by one of the collimators. The main primary collimators have aperture radii $3\,mm$. Optics A with sextupoles switched on.

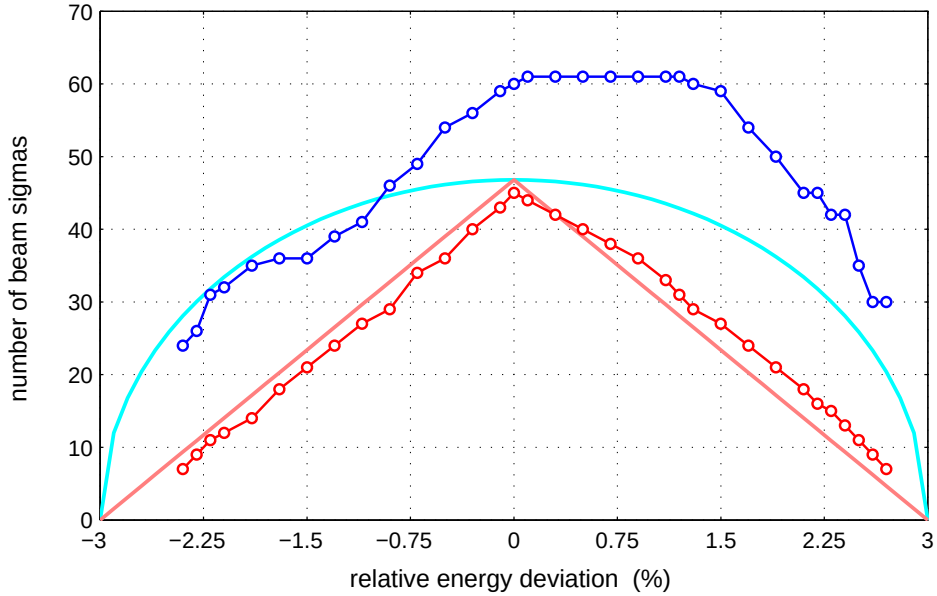

Figure 29: Minimal numbers of sigmas, n_x and n_y (red and blue curves), such that all particles, which have corresponding energy deviation and were able to pass the collimation system freely, lie inside $n_x\sigma_x$ and $n_y\sigma_y$ ellipses. Analytical estimates for n_x and n_y following from the linear theory are shown by pink and light-blue curves, respectively. The main primary collimators have aperture radii $3\,mm$. Optics A with sextupoles switched on.

It is not the subject of this paper to make a detailed study of the possibilities to protect the beam pipe inside the collimation section against impacts of primary particles. But, nevertheless, let us take a quick look at it, limiting ourselves to a consideration of incoming particles only from a 170-σ initial distribution with energy offsets within -15% and $+10\%$ limits. Fig.30 shows that the problem can not be solved simply by some reduction of the apertures of the main primary collimators, because the aperture radius required for the beam pipe protection not only becomes almost equal to zero for relatively large negative energy offsets, but also drops down in the neighbourhood of the nominal energy to about $0.2\,mm$. Fig.31 tells us that all particles which were able to hit the beam pipe between collimators are at large betatron amplitudes at the entrance of the collimation section. So one may intercept them using additional, suitably located collimators working at apertures larger than the apertures of the main collimators, and figs. 32 and 33 give an example showing that this really can be done.

8 Summary

The optics solution offered in this paper for the XFEL post-linac collimation section meets all design specifications. It is capable of providing simultaneously a large beam spot size at the collimator locations and, in the same time, to transport bunches with different energies (up to $\pm 1.5\%$ from nominal energy) while preserving with good accuracy energy independent input and output matching conditions. These criteria are met by designing a magnetic system whose second-order chromatic and geometric aberrations are controlled by the symmetry of the first-order optics and sextupole fields.

The system uses four main primary collimators and the studies presented in this paper show that these collimators are able to confine all particles which passed the collimation section freely (without touching collimator apertures) into a volume in the phase space, which can be safely transported through all downstream beamlines including undulator modules to the beam dumps.

In the next steps the set of exchangeable apertures (2 or 3 apertures) for the main primary collimators has to be defined, and the question concerning the number and locations of the supplementing primary collimators and secondary collimators has to be considered. Furthermore, the performance of the complete system in the presence of imperfections and with secondary and rescattered particles taken into account has to be studied.

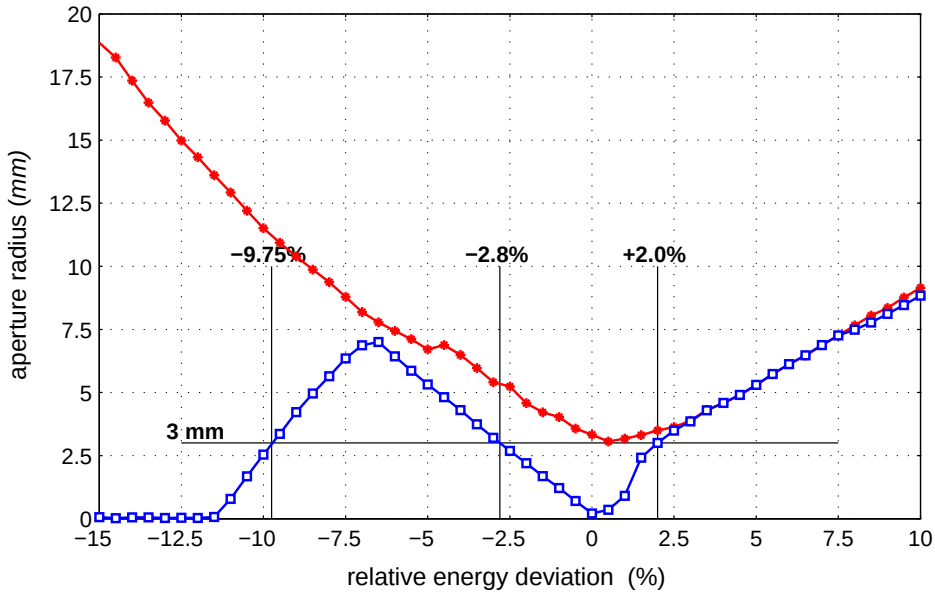

Figure 30: Red curve: aperture radius required to protect the undulator vacuum chamber ($r_{und} = 3\,mm$) as a function of the energy deviation. Blue curve: with additional requirement to have no uncontrolled losses of particles from initial 170-σ distribution on the beam pipe downstream of the first main collimator. Beam pipe radius is equal to $25\,mm$. Optics A with sextupoles switched on.

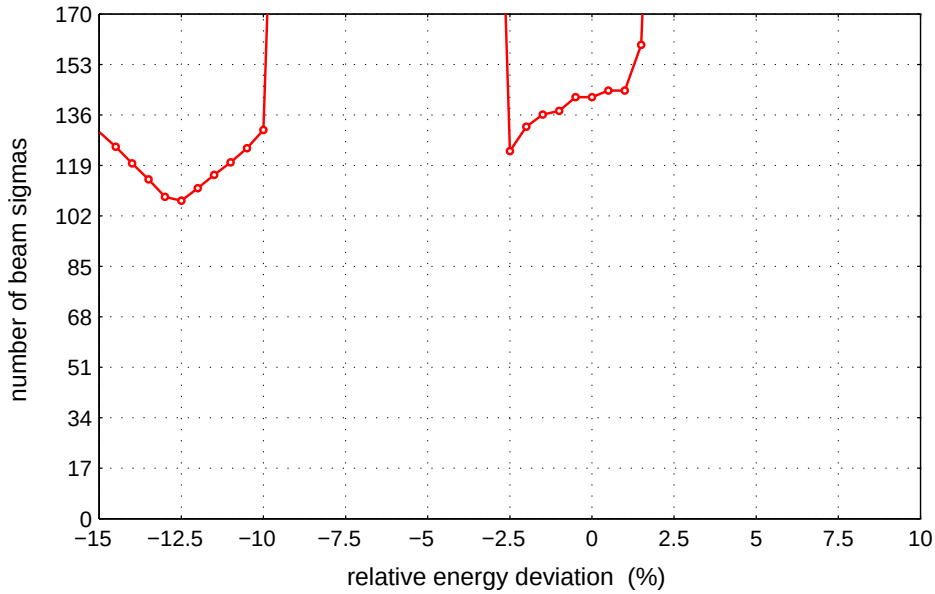

Figure 31: Number of sigmas (n) which separates corresponding monochromatic m-σ distributions into two classes: particles from all m-σ distributions with $m < n$ are not able to touch the beam pipe inside collimation section downstream of the first main collimator, but among particles from any m-σ distribution with $m > n$ there exists at least one particle whose trajectory will hit the vacuum chamber downstream of the first main collimator. The main collimators have aperture radii $3\,mm$. Beam pipe radius is equal to $25\,mm$. Optics A with sextupoles switched on.

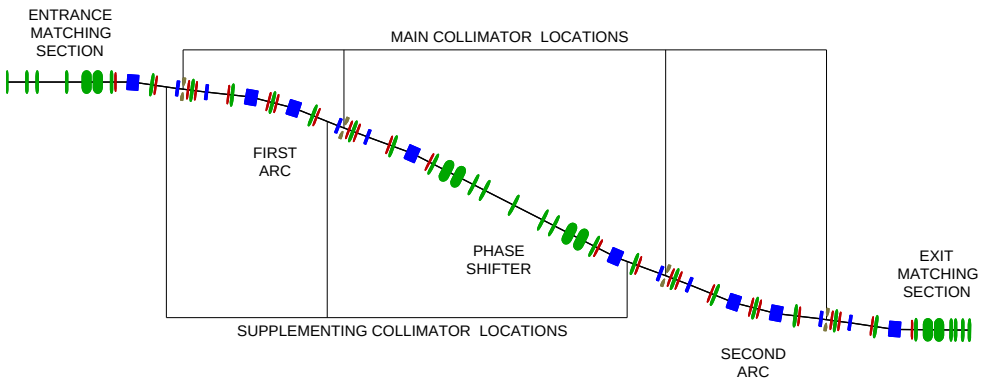

Figure 32: Example of location of three supplementing primary collimators in the XFEL post-linac collimation section.

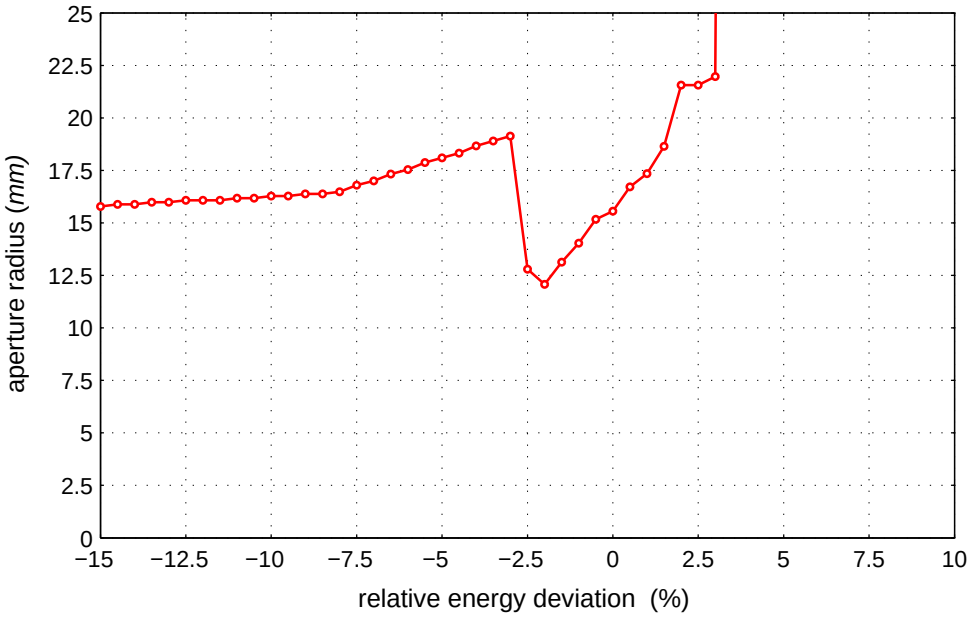

Figure 33: Aperture radius of the supplementing collimators (located as shown in fig. 32) required to protect the beam pipe downstream of the first supplementing collimator as a function of the energy deviation. Beam pipe radius is equal to 25 mm and the main collimators have aperture radii 3 mm. Optics A with sextupoles switched on.

A Equations of Motion and Transfer Matrices

Because various authors use various variables for the treatment of fully coupled transverse and longitudinal motion, the purpose of this appendix is to define exactly the variables and to write down equations of motion corresponding to these variables, which we use throughout this paper for analytical calculations and for numerical tracking. More details can be found in [18].

Besides that we bring together useful properties of transfer matrices of systems with symmetries collected from different literature [19, 20, 21, 22, 23].

A.1 Hamiltonian for the Motion of a Charged Particle in a Mid-Plane Symmetric Magnetic Field

As usual, we assume that the motion of a particle takes place in the vicinity of a given curve (reference orbit) which lies in the symmetry plane and use a set of curvilinear coordinates x, y, z of which the z-axis is tangent to this curve pointing in the direction of beam motion, x-axis lies in the symmetry plane and measures the distance normally from the reference orbit, and y-axis completes the set to form a right handed orthogonal coordinate system. When we take the path length along the reference orbit τ as independent variable, the Hamiltonian describing the motion of a particle can be written as

$$H(x,\, p_x,\, y,\, p_y,\, \sigma,\, \varepsilon) \;=$$

$$\varepsilon \;-\; (1+hx)\left(\sqrt{(1+\varepsilon)^2 - \left((p_x - A_x)^2 + (p_y - A_y)^2 + \left(\frac{\varepsilon}{\gamma_0}\right)^2\right)} \;+\; A_z\right), \qquad (4)$$

where $h(\tau)$ is the horizontal curvature of the reference orbit, measured as positive if the reference orbit bends in the direction opposite to that of the $x-$axis.

The canonical variable pairs are

$$(x,\, p_x), \quad (y,\, p_y), \quad (\sigma,\, \varepsilon), \qquad (5)$$

where p_x and p_y are transverse canonical monenta scaled with the constant kinetic momentum of the reference particle p_0.

The variables σ and ε which describe longitudinal dynamics are

$$\sigma \;=\; c\,\beta_0\,(t_0 \,-\, t) \;=\; v_0\,(t_0 \,-\, t) \qquad (6)$$

and

$$\varepsilon \;=\; \frac{1}{\beta_0^2}\cdot\frac{\mathcal{E} \,-\, \mathcal{E}_0}{\mathcal{E}_0} \;=\; \frac{1}{\beta_0^2}\cdot\frac{\gamma \,-\, \gamma_0}{\gamma_0} \;=\; \frac{1}{\beta_0^2}\cdot\frac{\beta_0\,|\,\vec{p}\,| \,-\, \beta\,p_0}{\beta\,p_0}\,. \qquad (7)$$

Here $\mathcal{E}_0$ and $t_0 = t_0(\tau)$ are the energy of the reference particle and its arrival time at certain position τ, and the values of p_0, γ_0 and β_0 are defined as follows

$$p_0 \;=\; \sqrt{\left(\frac{\mathcal{E}_0}{c}\right)^2 \;-\; m_0^2\,c^2} \;=\; m_0\,c\,\sqrt{\gamma_0^2 \;-\; 1} \;=\; m_0\,c\,\gamma_0\,\beta_0 \;=\; \frac{\beta_0\,\mathcal{E}_0}{c}\,. \tag{8}$$

Note that **variable σ is positive for particles which arrived at certain position τ before the reference particle, i.e. for the head of the bunch.**

To obtain a Taylor expansion of the Hamiltonian (4) one needs the Taylor expansions of the components of the magnetic vector potential A_x, A_y and A_z to be known. The coefficients in these expansions will depend on the coefficients in the magnetic field expansion but are not completely determined by them owing to the fact that one can add the gradient of an arbitrary scalar function to the vector potential without changing the magnetic field. In this paper we use the vector potential which satisfies additional gauge condition $A_y = 0$ and can be expanded as follows (for a more general discussion see, for example, [24])

$$A_x \;=_3\; k_0'\,\frac{x^2 - y^2}{2} \;+\; (k_1' - h k_0')\,\frac{x^3 - 3xy^2}{6} \;-\; (h' k_0 + 3h k_0')\,\frac{x^3}{6}\,, \tag{9}$$

$$A_y \;=_3\; 0\,, \tag{10}$$

and

$$A_z \;=_4\; -k_0\,x \;+\; h k_0\,\frac{x^2}{2} \;-\; k_1\,\frac{x^2 - y^2}{2} \;-\; k_2\,\frac{x^3 - 3xy^2}{6} \;+\; (k_0'' - 3h^2 k_0 + h k_1)\,\frac{x^3}{6} \;-$$

$$k_3\,\frac{x^4 - 6x^2y^2 + y^4}{24} \;+\; (k_1'' + h k_2 - h' k_0' - h^2 k_1 - 2h k_0'')\,\frac{x^4 - y^4}{24} \;+$$

$$(12h^3 k_0 - h'' k_0 - 6h k_0'' - 3h^2 k_1 - 4h' k_0')\,\frac{x^4}{24}\,. \tag{11}$$

Here $=_n$ means equality up to order n, prime denotes differentiation with respect to variable τ and multipole coefficients $k_n(\tau)$ are given by the following formula

$$k_n(\tau) \;=\; \frac{e}{p_0}\left(\frac{\partial^n B_y}{\partial x^n}\right)_{x=y=0}\,, \tag{12}$$

where $B_y = B_y(\tau, x, y)$ is the vertical component of the magnetic field vector.

With this particular form of the vector potential the expanded Hamiltonian becomes

$$H \;=_4\; H_1 \;+\; H_2 \;+\; H_3 \;+\; H_4\,, \tag{13}$$

where

$$H_1 \;=\; (k_0 \,-\, h)\, x\,, \tag{14}$$

$$H_2 \;=\; \frac{1}{2}\left(p_x^2 \,+\, p_y^2 \,+\, \left(\frac{\varepsilon}{\gamma_0}\right)^2\right) \;-\; hx\varepsilon \;+\; hk_0\,\frac{x^2}{2} \;+\; k_1\,\frac{x^2 \,-\, y^2}{2}\,, \tag{15}$$

$$H_3 \;=\; \frac{hx \,-\, \varepsilon}{2}\left(p_x^2 \,+\, p_y^2 \,+\, \left(\frac{\varepsilon}{\gamma_0}\right)^2\right) \;+\; k_2\,\frac{x^3 \,-\, 3xy^2}{6} \;-$$

$$k_0'\,\frac{x^2 p_x \,-\, p_x y^2}{2} \;-\; k_0''\,\frac{x^3}{6} \;+\; hk_1\,\frac{2x^3 \,-\, 3xy^2}{6}\,, \tag{16}$$

and

$$H_4 \;=\; \frac{1}{8}\left(p_x^2 \,+\, p_y^2 \,+\, \left(\frac{\varepsilon}{\gamma_0}\right)^2\right)^2 \;-\; \varepsilon\,\frac{hx \,-\, \varepsilon}{2}\left(p_x^2 \,+\, p_y^2 \,+\, \left(\frac{\varepsilon}{\gamma_0}\right)^2\right) \;+$$

$$k_3\,\frac{x^4 \,-\, 6x^2y^2 \,+\, y^4}{24} \;+\; \frac{1}{2}(k_0')^2\left(\frac{x^2 \,-\, y^2}{2}\right)^2 \;+\; (h'k_0 + 3hk_0')\frac{x^3 p_x}{6} \;-$$

$$(k_1' - hk_0')\,\frac{x^3 p_x \,-\, 3x p_x y^2}{6} \;+\; k_0'\,\frac{x^2 p_x \varepsilon \,-\, p_x y^2 \varepsilon}{2} \;-$$

$$hk_0'\,\frac{x^3 p_x \,-\, x p_x y^2}{2} \;-\; (k_1'' + hk_2 - h'k_0' - h^2 k_1 - 2hk_0'')\,\frac{x^4 \,-\, y^4}{24} \;+$$

$$hk_2\,\frac{x^4 \,-\, 3x^2y^2}{6} \;-\; (9h^3k_0 - 5hk_0'' - h''k_0 - 2h^2k_1 - 4h'k_0')\,\frac{x^4}{24}\,. \tag{17}$$

Note that throughout this paper we will also assume that $k_0(\tau) \equiv h(\tau)$ and that $h(\tau)\cdot k_n(\tau) \equiv 0$ for $n > 0$ (all magnets are separate function type).

A.2 Matrix of Static Magnetic System with Midplane Symmetry and its Dispersion Decomposition

The transfer matrix M_F of a magnetic system which is built from optical elements such that they are symmetric about the horizontal midplane $y = 0$ satisfy

$$T_M^{-1}\cdot M_F \cdot T_M \;=\; M_F\,, \tag{18}$$

where

$$T_M \;=\; T_M^{-1} \;=\; \begin{pmatrix} 1 & 0 & 0 & 0 & 0 & 0 \\ 0 & 1 & 0 & 0 & 0 & 0 \\ 0 & 0 & -1 & 0 & 0 & 0 \\ 0 & 0 & 0 & -1 & 0 & 0 \\ 0 & 0 & 0 & 0 & 1 & 0 \\ 0 & 0 & 0 & 0 & 0 & 1 \end{pmatrix} . \tag{19}$$

From (18), time-independence, energy conservation and symplecticity it follows that a matrix M_F of the static magnetic system which is symmetric about horizontal midplane has the following general form

$$M_F \;=\; \begin{pmatrix} r_{11} & r_{12} & 0 & 0 & 0 & r_{16} \\ r_{21} & r_{22} & 0 & 0 & 0 & r_{26} \\ 0 & 0 & r_{33} & r_{34} & 0 & 0 \\ 0 & 0 & r_{43} & r_{44} & 0 & 0 \\ r_{51} & r_{52} & 0 & 0 & 1 & r_{56} \\ 0 & 0 & 0 & 0 & 0 & 1 \end{pmatrix} , \tag{20}$$

where, due to symplecticity, the elements r_{nm} must satisfy

$$\begin{cases} r_{11}r_{22} - r_{12}r_{21} = 1 \\ r_{33}r_{44} - r_{34}r_{43} = 1 \\ r_{21}r_{16} - r_{11}r_{26} = r_{51} \\ r_{22}r_{16} - r_{12}r_{26} = r_{52} \\ r_{11}r_{52} - r_{12}r_{51} = r_{16} \\ r_{21}r_{52} - r_{22}r_{51} = r_{26} \end{cases} \tag{21}$$

The matrix elements r_{16} and r_{26} are called horizontal position and horizontal angular dispersions respectively.

If $tr_x = r_{11} + r_{22} \neq 2$ then the matrix M_F can be transformed into dispersion free form $N(M_F)$ with the help of the symplectic dispersion transformation $D(M_F)$

$$M_F \;=\; D(M_F) \cdot N(M_F) \cdot D(M_F)^{-1} . \tag{22}$$

Here

$$N(M_F) \;=\; \begin{pmatrix} r_{11} & r_{12} & 0 & 0 & 0 & 0 \\ r_{21} & r_{22} & 0 & 0 & 0 & 0 \\ 0 & 0 & r_{33} & r_{34} & 0 & 0 \\ 0 & 0 & r_{43} & r_{44} & 0 & 0 \\ 0 & 0 & 0 & 0 & 1 & C \\ 0 & 0 & 0 & 0 & 0 & 1 \end{pmatrix} , \tag{23}$$

$$D(M_F) \;=\; \begin{pmatrix} 1 & 0 & 0 & 0 & 0 & A \\ 0 & 1 & 0 & 0 & 0 & B \\ 0 & 0 & 1 & 0 & 0 & 0 \\ 0 & 0 & 0 & 1 & 0 & 0 \\ -B & A & 0 & 0 & 1 & 0 \\ 0 & 0 & 0 & 0 & 0 & 1 \end{pmatrix} \stackrel{\text{def}}{=} I \;+\; D_N(M_F)\,, \tag{24}$$

and

$$A \;=\; \frac{r_{16} - r_{52}}{2 - r_{11} - r_{22}}, \quad B \;=\; \frac{r_{26} + r_{51}}{2 - r_{11} - r_{22}}, \quad C \;=\; r_{56} + \frac{r_{16} r_{51} + r_{26} r_{52}}{2 - r_{11} - r_{22}}\,. \tag{25}$$

Because A and B defined by the above formulas satisfy

$$\begin{pmatrix} r_{11} & r_{12} \\ r_{21} & r_{22} \end{pmatrix} \cdot \begin{pmatrix} A \\ B \end{pmatrix} \;+\; \begin{pmatrix} r_{16} \\ r_{26} \end{pmatrix} \;=\; \begin{pmatrix} A \\ B \end{pmatrix}, \tag{26}$$

they are nothing else as initial conditions for periodic (matched) dispersion functions.

Note that the matrix $D_N(M_F)$ is nilpotent $(\, D_N(M_F)^2 \;=\; 0\,)$ and thus

$$D^{-1}(M_F) \;=\; (I + D_N(M_F))^{-1} \;=\; I - D_N(M_F)\,. \tag{27}$$

Note also that the dispersion transformation can be represented in the form of a Lie operator as follows

$$:\! D(M_F) \!: \;=\; exp(:\, \varepsilon \cdot (B \cdot x \;-\; A \cdot p_x)\, :)\,. \tag{28}$$

A.3 Matrix of Reversed Cell and Matrices of Two-Cell Systems

The matrix of the cell which is mirror symmetric about $x-y$ plane to the original (forward) cell is given by

$$M_R \;=\; T_R \cdot M_F^{-1} \cdot T_R\,, \tag{29}$$

where T_R is the reversion transformation matrix.

$$T_R \;=\; T_R^{-1} \;=\; \begin{pmatrix} 1 & 0 & 0 & 0 & 0 & 0 \\ 0 & -1 & 0 & 0 & 0 & 0 \\ 0 & 0 & 1 & 0 & 0 & 0 \\ 0 & 0 & 0 & -1 & 0 & 0 \\ 0 & 0 & 0 & 0 & -1 & 0 \\ 0 & 0 & 0 & 0 & 0 & 1 \end{pmatrix} \quad \text{and} \quad T_R^2 \;=\; I\,. \tag{30}$$

It should be noted that the reflection operation is involutory as would be expected, i.e.

$$(M_R)_R \;=\; T_R \cdot M_R^{-1} \cdot T_R \;=\; T_R \cdot (T_R \cdot M_F^{-1} \cdot T_R)^{-1} \cdot T_R \;=\; M_F\,. \tag{31}$$

If the forward cell is a magnetic system which is symmetric about horizontal midplane, then

$$M_R \;=\; \begin{pmatrix} r_{22} & r_{12} & 0 & 0 & 0 & -r_{52} \\ r_{21} & r_{11} & 0 & 0 & 0 & -r_{51} \\ 0 & 0 & r_{44} & r_{34} & 0 & 0 \\ 0 & 0 & r_{43} & r_{33} & 0 & 0 \\ -r_{26} & -r_{16} & 0 & 0 & 1 & r_{56} \\ 0 & 0 & 0 & 0 & 0 & 1 \end{pmatrix} . \tag{32}$$

Forward Cell Followed by Reversed Cell

Consider a magnet system with transfer matrix M_F followed by its mirror reflected system with transfer matrix M_R . For this combination one obtains

$$M_{FR} \stackrel{\text{def}}{=} M_R \cdot M_F \;=$$

$$\begin{pmatrix} 1+2r_{12}r_{21} & 2r_{12}r_{22} & 0 & 0 & 0 & 2r_{12}r_{26} \\ 2r_{21}r_{11} & 1+2r_{12}r_{21} & 0 & 0 & 0 & 2r_{11}r_{26} \\ 0 & 0 & 1+2r_{34}r_{43} & 2r_{34}r_{44} & 0 & 0 \\ 0 & 0 & 2r_{43}r_{33} & 1+2r_{34}r_{43} & 0 & 0 \\ -2r_{11}r_{26} & -2r_{12}r_{26} & 0 & 0 & 1 & 2(r_{56}-r_{16}r_{26}) \\ 0 & 0 & 0 & 0 & 0 & 1 \end{pmatrix} . \tag{33}$$

If one will consider this two-cell system as continuous system with the length of the forward cell equal to l_c , then the following relation holds

$$M_{FR}(l_c+\tau) \;=\; T_R \cdot M_{FR}(l_c-\tau) \cdot M_{FR}^{-1}(l_c) \cdot T_R \cdot M_{FR}(l_c)\,. \tag{34}$$

Let $\tilde{r}_{km}(\tau)$ be the elements of the matrix $M_{FR}(\tau) \cdot M_{FR}^{-1}(l_c)$. Rewriting (34) in the form

$$M_{FR}(l_c+\tau) \cdot M_{FR}^{-1}(l_c) \;=\; T_R \cdot \Big(M_{FR}(l_c-\tau) \cdot M_{FR}^{-1}(l_c)\Big) \cdot T_R \tag{35}$$

we have that

$$\tilde{r}_{11}, \quad \tilde{r}_{16}, \quad \tilde{r}_{22}, \quad \tilde{r}_{33}, \quad \tilde{r}_{44}, \quad \tilde{r}_{52} \tag{36}$$

are even and

$$\tilde{r}_{12}, \quad \tilde{r}_{21}, \quad \tilde{r}_{26}, \quad \tilde{r}_{34}, \quad \tilde{r}_{43}, \quad \tilde{r}_{51}, \quad \tilde{r}_{56} \tag{37}$$

are odd functions with respect to the point $\tau = l_c$.

Reversed Cell Followed by Forward Cell

$$M_{RF} \stackrel{\text{def}}{=} M_F \cdot M_R \; =$$

$$\begin{pmatrix} 1+2r_{12}r_{21} & 2r_{12}r_{11} & 0 & 0 & 0 & -2r_{12}r_{51} \\ 2r_{21}r_{22} & 1+2r_{12}r_{21} & 0 & 0 & 0 & -2r_{22}r_{51} \\ 0 & 0 & 1+2r_{34}r_{43} & 2r_{34}r_{33} & 0 & 0 \\ 0 & 0 & 2r_{43}r_{44} & 1+2r_{34}r_{43} & 0 & 0 \\ 2r_{22}r_{51} & 2r_{12}r_{51} & 0 & 0 & 1 & 2(r_{56}-r_{51}r_{52}) \\ 0 & 0 & 0 & 0 & 0 & 1 \end{pmatrix}. \quad (38)$$

Two-Periodic System

Two-periodic system is a repetition of two identical cells.

$$M_{FF} \stackrel{\text{def}}{=} M_F \cdot M_F \; =$$

$$\begin{pmatrix} r_{11}\,tr_x - 1 & r_{12}\,tr_x & 0 & 0 \\ r_{21}\,tr_x & r_{22}\,tr_x - 1 & 0 & 0 \\ 0 & 0 & r_{33}\,tr_y - 1 & r_{34}\,tr_y \\ 0 & 0 & r_{43}\,tr_y & r_{44}\,tr_y - 1 \\ (tr_x+1)r_{51} + r_{26} & (tr_x+1)r_{52} - r_{16} & 0 & 0 \\ 0 & 0 & 0 & 0 \end{pmatrix} \cdots$$

$$\cdots \begin{pmatrix} 0 & (tr_x+1)r_{16} - r_{52} \\ 0 & (tr_x+1)r_{26} + r_{51} \\ 0 & 0 \\ 0 & 0 \\ 1 & 2r_{56} + r_{16}r_{51} + r_{26}r_{52} \\ 0 & 1 \end{pmatrix}. \quad (39)$$

B Arc as Four-Cell Second-Order Achromat Based on Reflection Symmetry

One of the symmetries of arrangement of arc dipole and quadrupole magnets, which can be seen in fig.2 and which can be used in order to make the arc an achromat, is the four-cell symmetry of the type FRFR, where the forward cell is followed by reversed cell and then this two-cell configuration is repeated once more. According to the available theory, the minimum number of conditions required for

this system to become a second-order achromat are five for the first order and four for the second order [26, 27]. One of these first order constraints is that the angular dispersion, i.e. r_{26} matrix coefficient, is equal to zero in the end of the forward cell. In application to the arc design, this condition is somewhat too limiting, it makes our relatively simple system overconstrained, and in this appendix we will show that the requirement $r_{26} = 0$ is, in fact, superfluous[15]. Note that, similar to [26, 27], we will consider only magnetic systems with midplane symmetry.

B.1 First Order Requirements

The first-order conditions are that the system transfer matrix M_{arc} is equal to the identity matrix except, possibly, for the r_{56} element relating the time-of-flight difference to the energy difference between the reference particle and an off-energy particle.

Let us introduce the matrix $M_{FR} = M_R \cdot M_F$ with the elements $\bar{r}_{km}$ and write

$$M_{arc} = M_R \cdot M_F \cdot M_R \cdot M_F = (M_R \cdot M_F)_R \cdot (M_R \cdot M_F)_F =$$

$$(M_{FR})_R \cdot (M_{FR})_F \,. \tag{40}$$

Applying now formulae (33) to the product in the right hand side of (40) we obtain that to satisfy the first order requirements one must have

$$\bar{r}_{12} = \bar{r}_{21} = \bar{r}_{26} = \bar{r}_{34} = \bar{r}_{43} = 0 \,. \tag{41}$$

Resolving now the equations (41) in the terms of the elements of the forward cell matrix M_F we obtain two solutions for the x-motion

$$r_{12} = r_{21} = r_{26} = 0 \quad \text{or} \quad r_{11} = r_{22} = 0 \,, \tag{42}$$

and also two solutions for the y-motion

$$r_{34} = r_{43} = 0 \quad \text{or} \quad r_{33} = r_{44} = 0 \,. \tag{43}$$

Note that because

$$(M_{FR})_R = (M_{FR})_F \,, \tag{44}$$

the arc matrix M_{arc} can also be written as

$$M_{arc} = (M_{FR})_F \cdot (M_{FR})_R \,, \tag{45}$$

[15]Note that the fact, that instead of five first order conditions only four are really necessary, is true in application to some other four-cell systems considered in [26, 27].

and one can use formulae (38) instead of (33) and obtain

$$\bar{r}_{12} \;=\; \bar{r}_{21} \;=\; \bar{r}_{51} \;=\; \bar{r}_{34} \;=\; \bar{r}_{43} \;=\; 0\,, \tag{46}$$

which is equivalent to (41) due to symplecticity conditions (21). Even more, using (44) one may recover the same conditions (42)-(43) starting from repetitive symmetry

$$M_{arc} \;=\; (M_{FR})_F \cdot (M_{FR})_F\,, \tag{47}$$

but calculations along this road will take a little bit longer.

With the second sets from conditions (42) and (43) satisfied[16] the matrix of one half of the arc takes the form

$$M_{FR} \;=\; \begin{pmatrix} -1 & 0 & 0 & 0 & 0 & 2r_{12}r_{26} \\ 0 & -1 & 0 & 0 & 0 & 0 \\ 0 & 0 & -1 & 0 & 0 & 0 \\ 0 & 0 & 0 & -1 & 0 & 0 \\ 0 & -2r_{12}r_{26} & 0 & 0 & 1 & 2(r_{56}-r_{16}r_{26}) \\ 0 & 0 & 0 & 0 & 0 & 1 \end{pmatrix} \tag{48}$$

and, as it was required

$$M_{arc} \;=\; \begin{pmatrix} 1 & 0 & 0 & 0 & 0 & 0 \\ 0 & 1 & 0 & 0 & 0 & 0 \\ 0 & 0 & 1 & 0 & 0 & 0 \\ 0 & 0 & 0 & 1 & 0 & 0 \\ 0 & 0 & 0 & 0 & 1 & 4(r_{56}-r_{16}r_{26}) \\ 0 & 0 & 0 & 0 & 0 & 1 \end{pmatrix}. \tag{49}$$

Thus, to construct a four-cell second-order achromat using reflection symmetry, not simply a 90° cell is needed as in an achromat built out of four identical cells, but a 90° cell with zero diagonal elements

$$r_{11} \;=\; r_{22} \;=\; r_{33} \;=\; r_{44} \;=\; 0\,. \tag{50}$$

B.2 Second Order Requirements

The second order aberrations of the transfer map $:\mathcal{M}_{\mathcal{F}}:$ of the first cell of the arc (forward cell) can be represented by a matrix M_F and a third order polynomial $\mathcal{F}_3$ through a Lie factorization as (see, for example, [25])

$$:\mathcal{M}_{\mathcal{F}}: =_2 \; \exp(:\mathcal{F}_3(\boldsymbol{z}):) : M_F :\,, \tag{51}$$

[16]The first sets of conditions (42) and (43) mean that the matrix of one half of the arc is already an identity matrix and are not interesting for us in this paper.

where $=_2$ denotes equality up to order 2 when maps on both sides of (51) are applied to the phase space vector $\boldsymbol{z}$.

The map of the cell in which the order of the magnetic elements is reversed from that of the forward cell (reversed cell) is given by the following Lie factorization

$$: \mathcal{M}_{\mathcal{R}} : = : T_R :: \mathcal{M}_{\mathcal{F}} :^{-1}: T_R : =_2 : M_R : \exp(: \mathcal{F}_3(T_R \cdot \boldsymbol{z}) :) \,. \tag{52}$$

Thus the transfer map $: \mathcal{M}_{arc} :$ of the total arc considered as four-cell system is given by

$$: \mathcal{M}_{arc} : = : \mathcal{M}_{\mathcal{F}} :: \mathcal{M}_{\mathcal{R}} :: \mathcal{M}_{\mathcal{F}} :: \mathcal{M}_{\mathcal{R}} : =_2 \; \exp(: \mathcal{F}_3(\boldsymbol{z}) :) : M_F :$$

$$: M_R : \exp(: \mathcal{F}_3(T_R \cdot \boldsymbol{z}) :) \exp(: \mathcal{F}_3(\boldsymbol{z}) :) : M_F :: M_R : \exp(: \mathcal{F}_3(T_R \cdot \boldsymbol{z}) :) \; =_2$$

$$\exp(: \mathcal{F}_3(\boldsymbol{z}) :) : M_{FR} : \exp(: \mathcal{F}_3(\boldsymbol{z}) + \mathcal{F}_3(T_R \cdot \boldsymbol{z}) :) : M_{FR} : \exp(: \mathcal{F}_3(T_R \cdot \boldsymbol{z}) :) \,. \tag{53}$$

Dispersion decomposition (22) applied to the matrix M_{FR} which has the form (48) gives

$$: M_{FR} : = : D(M_{FR}) \cdot N(M_{FR}) \cdot D^{-1}(M_{FR}) : =$$

$$: D(M_{FR}) :^{-1}: N(M_{FR}) :: D(M_{FR}) : \tag{54}$$

with coefficients A, B and C defined as follows

$$A \; = \; r_{12} r_{26} \; = \; -r_{52} \,, \quad B \; = \; 0 \,, \quad C \; = \; 2\,(r_{56} - r_{16} r_{26}) \,. \tag{55}$$

Substituting (54) into (53) we obtain after some straightforward manipulations

$$: \mathcal{M}_{arc} : =_2 : D(M_{FR}) :^{-1} \exp(: \mathcal{K}_3(\boldsymbol{z}) :) : N^2(M_{FR}) :: D(M_{FR}) : \tag{56}$$

where

$$\mathcal{K}_3(\boldsymbol{z}) \; = \; \mathcal{F}_3(D(M_{FR}) \cdot \boldsymbol{z}) \; + \; \mathcal{F}_3(D(M_{FR}) N(M_{FR}) \cdot \boldsymbol{z}) \; +$$

$$\mathcal{F}_3(T_R D(M_{FR}) N(M_{FR}) \cdot \boldsymbol{z}) \; + \; \mathcal{F}_3(T_R D(M_{FR}) N^2(M_{FR}) \cdot \boldsymbol{z}) \,. \tag{57}$$

Because $B = 0$, the matrices T_R and $D(M_{FR})$ commute, i.e.

$$T_R \cdot D(M_{FR}) \; = \; D(M_{FR}) \cdot T_R \,, \tag{58}$$

and we can rewrite (57) as

$$\mathcal{K}_3(\boldsymbol{z}) \; = \; \mathcal{F}_3(D(M_{FR}) \cdot (\boldsymbol{z})) \; + \; \mathcal{F}_3(D(M_{FR}) \cdot (N(M_{FR}) \cdot \boldsymbol{z})) \; +$$

$$\mathcal{F}_3(D(M_{FR})\cdot(T_R N(M_{FR})\cdot\boldsymbol{z}))\ +\ \mathcal{F}_3(D(M_{FR})\cdot(T_R N^2(M_{FR})\cdot\boldsymbol{z}))\,, \tag{59}$$

which is equivalent to

$$\mathcal{K}_3(\boldsymbol{z})\ =\ \mathcal{P}_3(\boldsymbol{z})\ +\ \mathcal{P}_3(N(M_{FR})\cdot\boldsymbol{z})\ +$$

$$\mathcal{P}_3(T_R N(M_{FR})\cdot\boldsymbol{z})\ +\ \mathcal{P}_3(T_R N^2(M_{FR})\cdot\boldsymbol{z})\ =$$

$$\mathcal{P}_3(x,\,p_x,\,y,\,p_y,\,\varepsilon)\ +\ \mathcal{P}_3(-x,\,-p_x,\,-y,\,-p_y,\,\varepsilon)\ +$$

$$\mathcal{P}_3(-x,\,p_x,\,-y,\,p_y,\,\varepsilon)\ +\ \mathcal{P}_3(x,\,-p_x,\,y,\,-p_y,\,\varepsilon)\,, \tag{60}$$

where $\mathcal{P}_3$ is defined as

$$\mathcal{P}_3(\boldsymbol{z})\ =\ \mathcal{F}_3(D(M_{FR})\cdot\boldsymbol{z})\ =\ \mathcal{F}_3(x-r_{52}\varepsilon,\,p_x,\,y,\,p_y,\,\varepsilon)\,. \tag{61}$$

Let $c_{abcde}(\mathcal{P}_3)$ be the coefficient with which monomial $x^a\,p_x^b\,y^c\,p_y^d\,\varepsilon^e$ enters the polynomial $\mathcal{P}_3$. Then (60) can be rewritten as

$$\mathcal{K}_3(\boldsymbol{z})\ =\ 4\varepsilon\cdot\Big(c_{20001}(\mathcal{P}_3)\cdot x^2\ +\ c_{02001}(\mathcal{P}_3)\cdot p_x^2\ +\ c_{00201}(\mathcal{P}_3)\cdot y^2\ +$$

$$c_{00021}(\mathcal{P}_3)\cdot p_y^2\ +\ c_{10101}(\mathcal{P}_3)\cdot xy\ +\ c_{01011}(\mathcal{P}_3)\cdot p_x p_y\ +\ c_{00003}(\mathcal{P}_3)\cdot\varepsilon^2\Big)\,, \tag{62}$$

or, when expressed using coefficients of polynomial $\mathcal{F}_3$,

$$\mathcal{K}_3(\boldsymbol{z})\ =\ 4\varepsilon\cdot\Big((c_{20001}(\mathcal{F}_3)\ -\ 3r_{52}\cdot c_{30000}(\mathcal{F}_3))\cdot x^2\ +$$

$$(c_{02001}(\mathcal{F}_3)\ -\ r_{52}\cdot c_{12000}(\mathcal{F}_3))\cdot p_x^2\ +$$

$$(c_{00201}(\mathcal{F}_3)\ -\ r_{52}\cdot c_{10200}(\mathcal{F}_3))\cdot y^2\ +$$

$$(c_{00021}(\mathcal{F}_3)\ -\ r_{52}\cdot c_{10020}(\mathcal{F}_3))\cdot p_y^2\ +$$

$$(c_{10101}(\mathcal{F}_3)\ -\ 2r_{52}\cdot c_{20100}(\mathcal{F}_3))\cdot xy\ +$$

$$(c_{01011}(\mathcal{F}_3)\ -\ r_{52}\cdot c_{11010}(\mathcal{F}_3))\cdot p_x p_y\ +$$

$$\Big(c_{00003}(\mathcal{F}_3)\ -\ r_{52}\cdot c_{10002}(\mathcal{F}_3)\ +\ r_{52}^2\cdot c_{20001}(\mathcal{F}_3)\ -\ r_{52}^3\cdot c_{30000}(\mathcal{F}_3)\Big)\cdot\varepsilon^2\Big)\,. \tag{63}$$

Representing now the operator $: N^2(M_{FR}) :$ in exponential form

$$: N^2(M_{FR}) : = \ exp(: 2(r_{56} - r_{16}r_{26}) \cdot \varepsilon^2 :) \tag{64}$$

and taking into account that

$$: N^2(M_{FR}) :: D(M_{FR}) : = : D(M_{FR}) :: N^2(M_{FR}) : \tag{65}$$

we obtain from (56) the representation of the first and second order terms of the arc map in the form of a single Lie exponent

$$: \mathcal{M}_{arc} : =_2 \ \exp(: \mathcal{K}_3(x + r_{52} \cdot \varepsilon, p_x, y, p_y, \varepsilon) + 2(r_{56} - r_{16}r_{26}) \cdot \varepsilon^2 :) \,, \tag{66}$$

which has the advantage of explicitly showing the number of independent aberrations to be corrected.

For a system consisting of only magnets with the mid-plane symmetry, $\mathcal{F}_3$ is an even function of variables y and p_y, which yields,

$$c_{10101}(\mathcal{F}_3) \ = \ c_{20100}(\mathcal{F}_3) \ = \ c_{01011}(\mathcal{F}_3) \ = \ c_{11010}(\mathcal{F}_3) \ = \ 0 \,, \tag{67}$$

and only 4 conditions

$$\left\{ \begin{array}{rcrcrcl} c_{20001}(\mathcal{K}_3) & = & 4 \cdot (c_{20001}(\mathcal{F}_3) & - & 3r_{52} \cdot c_{30000}(\mathcal{F}_3)) & = & 0 \\ c_{02001}(\mathcal{K}_3) & = & 4 \cdot (c_{02001}(\mathcal{F}_3) & - & r_{52} \cdot c_{12000}(\mathcal{F}_3)) & = & 0 \\ c_{00201}(\mathcal{K}_3) & = & 4 \cdot (c_{00201}(\mathcal{F}_3) & - & r_{52} \cdot c_{10200}(\mathcal{F}_3)) & = & 0 \\ c_{00021}(\mathcal{K}_3) & = & 4 \cdot (c_{00021}(\mathcal{F}_3) & - & r_{52} \cdot c_{10020}(\mathcal{F}_3)) & = & 0 \end{array} \right. \tag{68}$$

remain to be satisfied to achieve a second order achromat, which, in general, requires 4 independent sextupole families.

B.3 Second Order Aberrations as Integrals of First-Order Trajectories

It is useful to express the second-order aberrations as integrals of the first-order trajectories (matrix elements) and of the magnetic field parameters (multipole components). Using

$$\mathcal{F}_3(\boldsymbol{z}) \ = \ -\int_0^{l_c} H_3(\tau, \ M_F(\tau) \cdot \boldsymbol{z}) \, d\tau \tag{69}$$

where $H_3(\tau, \boldsymbol{z})$ is given by (16) and l_c is the length of the forward cell, and introducing notations

$$D_0(\tau) \ = \ r_{16}(\tau) \ - \ r_{52}(l_c) \cdot r_{11}(\tau) \tag{70}$$

and

$$D_0'(\tau) \;=\; r_{26}(\tau) \;-\; r_{52}(l_c)\cdot r_{21}(\tau) \tag{71}$$

we obtain after some straightforward manipulations

$$c_{20001}(\mathcal{K}_3) \;=\; -2\int_0^{l_c}\Big(k_2 r_{11}^2 D_0 \;+\; 2h r_{11} r_{21} D_0' \;+\; h r_{21}^2 D_0 \;-$$

$$2h' r_{11} r_{21} D_0 \;-\; h' r_{11}^2 D_0' \;-\; h'' r_{11}^2 D_0 \;+\; 2hk_1 r_{11}^2 D_0 \;-\; r_{21}^2\Big)\, d\tau \;=$$

$$-2\int_0^{l_c}\Big(k_2 r_{11}^2 D_0 + h\left(r_{11}^2\right)' D_0' + h r_{21}^2 D_0 - \left(h' r_{11}^2 D_0\right)' + 2hk_1 r_{11}^2 D_0 - r_{21}^2\Big)\, d\tau \;=$$

$$-2\int_0^{l_c}\Big(k_2 r_{11}^2 D_0 \;+\; h\left(r_{11}^2\right)' D_0' \;+\; h r_{21}^2 D_0 \;+\; 2hk_1 r_{11}^2 D_0 \;-\; r_{21}^2\Big)\, d\tau\,, \tag{72}$$

$$c_{02001}(\mathcal{K}_3) \;=\; -2\int_0^{l_c}\Big(k_2 r_{12}^2 D_0 \;+\; 2h r_{12} r_{22} D_0' \;+\; h r_{22}^2 D_0 \;-$$

$$2h' r_{12} r_{22} D_0 \;-\; h' r_{12}^2 D_0' \;-\; h'' r_{12}^2 D_0 \;+\; 2hk_1 r_{12}^2 D_0 \;-\; r_{22}^2\Big)\, d\tau \;=$$

$$-2\int_0^{l_c}\Big(k_2 r_{12}^2 D_0 + h\left(r_{12}^2\right)' D_0' + h r_{22}^2 D_0 - \left(h' r_{12}^2 D_0\right)' + 2hk_1 r_{12}^2 D_0 - r_{22}^2\Big)\, d\tau \;=$$

$$-2\int_0^{l_c}\Big(k_2 r_{12}^2 D_0 \;+\; h\left(r_{12}^2\right)' D_0' \;+\; h r_{22}^2 D_0 \;+\; 2hk_1 r_{12}^2 D_0 \;-\; r_{22}^2\Big)\, d\tau\,, \tag{73}$$

$$c_{00201}(\mathcal{K}_3) \;=\; 2\int_0^{l_c}\Big(k_2 r_{33}^2 D_0 - h r_{43}^2 D_0 - h' r_{33}^2 D_0' + hk_1 r_{33}^2 D_0 + r_{43}^2\Big)\, d\tau\,, \tag{74}$$

$$c_{00021}(\mathcal{K}_3) \;=\; 2\int_0^{l_c}\Big(k_2 r_{34}^2 D_0 - h r_{44}^2 D_0 - h' r_{34}^2 D_0' + hk_1 r_{34}^2 D_0 + r_{44}^2\Big)\, d\tau\,. \tag{75}$$

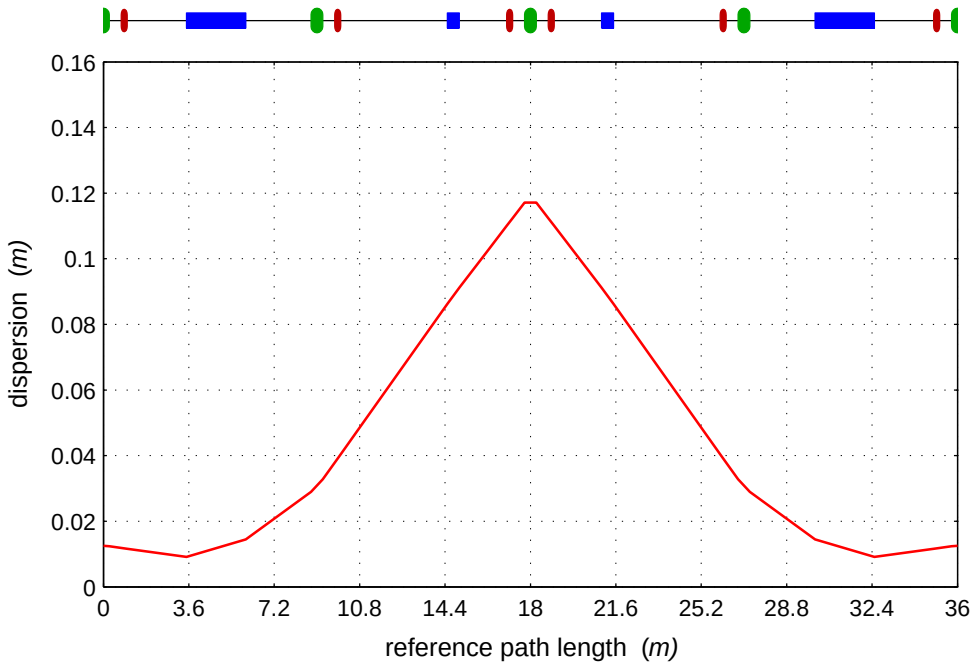

Figure 34: Solution for dispersion which is periodic for the first half of the first arc of the XFEL post-linac collimation section.

Note that in deriving formulas (72) and (73) we have used the equalities

$$\int_0^{l_c} \left(h' r_{11}^2 D_0\right)' d\tau \;=\; \int_0^{l_c} \left(h' r_{12}^2 D_0\right)' d\tau \;=\; 0\,,$$

which, in general, are not true for an arbitrary cell, but must be satisfied for the cell which is the forward cell of some FRFR system.

Note also that, in contrast with repetitive achromat theories, the dispersion D_0 in (72)-(75) is not the periodic (matched) cell dispersion, but is the dispersion which is periodic for the system which consist of forward cell followed by reversed cell and, in application to the arc design, can be seen in fig.34.

C Arc as Two-Cell Second-Order Achromat Based on Repetitive Symmetry

In contrast to the case discussed above, another symmetry (which also can be seen in fig.2) can be used in order to make the arc an achromat: consider the arc as a repetition of two identical cells. The repetitive second-order achromats were the first achromats ever considered [28], and the importance of the achromat concept is

now well established and was used in the design of many particle accelerators and beam transport lines (see, for example, [29]).

The theory of repetitive achromats (see, for example, [30]) states, that a system built out of n identical cells ($n > 1$) with the overall first order matrix equaling to unity in both transverse planes and with the tunes of a cell such that resonances which are not forbidden by the mid-plane symmetry are avoided up to third order, cancels all second-order geometric aberrations and can be corrected to become a second-order achromat using only two families of sextupoles.

This theory relies on appropriate selection of cell tunes in order to cancel all geometric aberrations and in order to reduce the number of independent chromatic aberrations to two and, therefore, the number of cells must be greater or equal to four.

It is also known that, in the case n is equal to two and cell tunes are not integers, geometric aberrations are still cancelled automatically, but the number of independent chromatic aberrations becomes larger than two and can not be cancelled by using only two families of sextupoles. It is, probably, the main reason why we were not able to find in the literature an accurate consideration of two-cell second-order achromats (though there is an example of a constructed and operated "practical" two-cell second-order achromat [31]) and in this appendix we fill this unexpected gap in the achromat theories.

C.1 First Order Requirements

The matrix of the arc M_{arc} considered as a repetition of two identical cells satisfies

$$M_{arc} \;=\; M_{\mathcal{H}} \cdot M_{\mathcal{H}}\,, \tag{76}$$

where $M_{\mathcal{H}}$ is the matrix of the half of the arc and its elements we will denote as $\bar{r}_{km}$. Applying now formulae (39) to the product in the right hand side of (76) we obtain two solutions for the x-motion

$$\left\{\begin{array}{rcl} \bar{r}_{12} &=& 0 \\ \bar{r}_{21} &=& 0 \\ \bar{r}_{16} &=& 0 \\ \bar{r}_{26} &=& 0 \\ \bar{r}_{11} &=& 1 \\ \bar{r}_{22} &=& 1 \end{array}\right. \quad \text{or} \quad \left\{\begin{array}{rcl} \bar{r}_{12} &=& 0 \\ \bar{r}_{21} &=& 0 \\ \bar{r}_{11} &=& -1 \\ \bar{r}_{22} &=& -1 \end{array}\right. \tag{77}$$

and also two solutions for the y-motion

$$\left\{\begin{array}{rcl} \bar{r}_{34} &=& 0 \\ \bar{r}_{43} &=& 0 \\ \bar{r}_{33} &=& 1 \\ \bar{r}_{44} &=& 1 \end{array}\right. \quad \text{or} \quad \left\{\begin{array}{rcl} \bar{r}_{34} &=& 0 \\ \bar{r}_{43} &=& 0 \\ \bar{r}_{33} &=& -1 \\ \bar{r}_{44} &=& -1 \end{array}\right. \tag{78}$$

among which one can choose in order to satisfy the first order requirements, which are the same as for the symmetry FRFR considered in the previous appendix.

With the second sets from conditions (77) and (78) satisfied[17], the matrix of the half of the arc takes the form

$$M_{\mathcal{H}} \;=\; \begin{pmatrix} -1 & 0 & 0 & 0 & 0 & \bar{r}_{16} \\ 0 & -1 & 0 & 0 & 0 & \bar{r}_{26} \\ 0 & 0 & -1 & 0 & 0 & 0 \\ 0 & 0 & 0 & -1 & 0 & 0 \\ \bar{r}_{26} & -\bar{r}_{16} & 0 & 0 & 1 & \bar{r}_{56} \\ 0 & 0 & 0 & 0 & 0 & 1 \end{pmatrix} \tag{79}$$

and, as it was required

$$M_{arc} \;=\; \begin{pmatrix} 1 & 0 & 0 & 0 & 0 & 0 \\ 0 & 1 & 0 & 0 & 0 & 0 \\ 0 & 0 & 1 & 0 & 0 & 0 \\ 0 & 0 & 0 & 1 & 0 & 0 \\ 0 & 0 & 0 & 0 & 1 & 2\bar{r}_{56} \\ 0 & 0 & 0 & 0 & 0 & 1 \end{pmatrix} . \tag{80}$$

C.2 Second Order Requirements

If we will assume that

$$: \mathcal{M}_{\mathcal{H}} : =_2 \; \exp(: \mathcal{L}_3(\boldsymbol{z}) :) : M_{\mathcal{H}} : \tag{81}$$

is the transfer map of the half of the arc, then the transfer map of the total arc considered as two-cell system is given by

$$: \mathcal{M}_{arc} : = : \mathcal{M}_{\mathcal{H}} :: \mathcal{M}_{\mathcal{H}} : =_2 \exp(: \mathcal{L}_3(\boldsymbol{z}) :) : M_{\mathcal{H}} : \exp(: \mathcal{L}_3(\boldsymbol{z}) :) : M_{\mathcal{H}} : \; . \tag{82}$$

Dispersion decomposition (22) of the matrix $M_{\mathcal{H}}$ of the form (79) yields

$$A \;=\; \frac{\bar{r}_{16}}{2}, \quad B \;=\; \frac{\bar{r}_{26}}{2}, \quad C \;=\; \bar{r}_{56} \tag{83}$$

and when substituted into (82) gives after some straightforward manipulations

$$: \mathcal{M}_{arc} : =_2 : D(M_{\mathcal{H}}) :^{-1} \exp(: \mathcal{Q}_3(\boldsymbol{z}) :) : N^2(M_{\mathcal{H}}) :: D(M_{\mathcal{H}}) : , \tag{84}$$

where

$$\mathcal{Q}_3(\boldsymbol{z}) \;=\; \mathcal{L}_3(D(M_{\mathcal{H}}) \cdot (\boldsymbol{z})) \;+\; \mathcal{L}_3(D(M_{\mathcal{H}}) \cdot (N(M_{\mathcal{H}}) \cdot \boldsymbol{z})) \, . \tag{85}$$

[17]The first sets of conditions (77) and (78), as in the case of the symmetry FRFR, mean that the matrix of the half of the arc is already an identity matrix and again are not interesting for us in this paper.

With midplane symmetry taken into account the polynomial $\mathcal{Q}_3$ can be expressed using coefficients of the polynomial $\mathcal{L}_3$ as follows

$$\begin{aligned}\mathcal{Q}_3(\boldsymbol{z}) = 2\varepsilon \cdot \Bigg(\Big(& c_{20001}(\mathcal{L}_3) \;+\; \frac{3}{2}\,\bar{r}_{16} \cdot c_{30000}(\mathcal{L}_3) \;+\; \frac{1}{2}\,\bar{r}_{26} \cdot c_{21000}(\mathcal{L}_3) \Big) \cdot x^2 \;+ \\ & \Big(c_{02001}(\mathcal{L}_3) \;+\; \frac{3}{2}\,\bar{r}_{26} \cdot c_{03000}(\mathcal{L}_3) \;+\; \frac{1}{2}\,\bar{r}_{16} \cdot c_{12000}(\mathcal{L}_3) \Big) \cdot p_x^2 \;+ \\ & \big(c_{11001}(\mathcal{L}_3) \;+\; \bar{r}_{16} \cdot c_{21000}(\mathcal{L}_3) \;+\; \bar{r}_{26} \cdot c_{12000}(\mathcal{L}_3) \big) \cdot x p_x \;+ \\ & \Big(c_{00201}(\mathcal{L}_3) \;+\; \frac{1}{2}\,\bar{r}_{16} \cdot c_{10200}(\mathcal{L}_3) \;+\; \frac{1}{2}\,\bar{r}_{26} \cdot c_{01200}(\mathcal{L}_3) \Big) \cdot y^2 \;+ \\ & \Big(c_{00021}(\mathcal{L}_3) \;+\; \frac{1}{2}\,\bar{r}_{16} \cdot c_{10020}(\mathcal{L}_3) \;+\; \frac{1}{2}\,\bar{r}_{26} \cdot c_{01020}(\mathcal{L}_3) \Big) \cdot p_y^2 \;+ \\ & \Big(c_{00111}(\mathcal{L}_3) \;+\; \frac{1}{2}\,\bar{r}_{16} \cdot c_{10110}(\mathcal{L}_3) \;+\; \frac{1}{2}\,\bar{r}_{26} \cdot c_{01110}(\mathcal{L}_3) \Big) \cdot y p_y \;+ \\ & \Big(c_{00003}(\mathcal{L}_3) \;+\; \frac{1}{2}\,\bar{r}_{16} \cdot c_{10002}(\mathcal{L}_3) \;+\; \frac{1}{2}\,\bar{r}_{26} \cdot c_{01002}(\mathcal{L}_3) \;+\; \frac{1}{4}\,\bar{r}_{16}^2 \cdot c_{20001}(\mathcal{L}_3) \;+ \\ & \frac{1}{4}\,\bar{r}_{16}\,\bar{r}_{26} \cdot c_{11001}(\mathcal{L}_3) \;+\; \frac{1}{4}\,\bar{r}_{26}^2 \cdot c_{02001}(\mathcal{L}_3) \;+\; \frac{1}{8}\,\bar{r}_{16}^3 \cdot c_{30000}(\mathcal{L}_3) \;+ \\ & \frac{1}{8}\,\bar{r}_{16}^2\,\bar{r}_{26} \cdot c_{21000}(\mathcal{L}_3) \;+\; \frac{1}{8}\,\bar{r}_{16}\,\bar{r}_{26}^2 \cdot c_{12000}(\mathcal{L}_3) \;+\; \frac{1}{8}\,\bar{r}_{26}^3 \cdot c_{03000}(\mathcal{L}_3) \Big) \cdot \varepsilon^2 \Big) \,, \end{aligned} \tag{86}$$

and that gives us 6 conditions

$$\begin{cases} c_{20001}(\mathcal{Q}_3) = 2 \cdot (c_{20001}(\mathcal{L}_3) \;+\; \frac{3}{2}\bar{r}_{16} \cdot c_{30000}(\mathcal{L}_3) \;+\; \frac{1}{2}\bar{r}_{26} \cdot c_{21000}(\mathcal{L}_3)) \;=\; 0 \\ c_{02001}(\mathcal{Q}_3) = 2 \cdot (c_{02001}(\mathcal{L}_3) \;+\; \frac{3}{2}\bar{r}_{26} \cdot c_{03000}(\mathcal{L}_3) \;+\; \frac{1}{2}\bar{r}_{16} \cdot c_{12000}(\mathcal{L}_3)) \;=\; 0 \\ c_{11001}(\mathcal{Q}_3) = 2 \cdot (c_{11001}(\mathcal{L}_3) \;+\; \bar{r}_{16} \cdot c_{21000}(\mathcal{L}_3) \;+\; \bar{r}_{26} \cdot c_{12000}(\mathcal{L}_3)) \;=\; 0 \\ c_{00201}(\mathcal{Q}_3) = 2 \cdot (c_{00201}(\mathcal{L}_3) \;+\; \frac{1}{2}\bar{r}_{16} \cdot c_{10200}(\mathcal{L}_3) \;+\; \frac{1}{2}\bar{r}_{26} \cdot c_{01200}(\mathcal{L}_3)) \;=\; 0 \\ c_{00021}(\mathcal{Q}_3) = 2 \cdot (c_{00021}(\mathcal{L}_3) \;+\; \frac{1}{2}\bar{r}_{16} \cdot c_{10020}(\mathcal{L}_3) \;+\; \frac{1}{2}\bar{r}_{26} \cdot c_{01020}(\mathcal{L}_3)) \;=\; 0 \\ c_{00111}(\mathcal{Q}_3) = 2 \cdot (c_{00111}(\mathcal{L}_3) \;+\; \frac{1}{2}\bar{r}_{16} \cdot c_{10110}(\mathcal{L}_3) \;+\; \frac{1}{2}\bar{r}_{26} \cdot c_{01110}(\mathcal{L}_3)) \;=\; 0 \end{cases} \tag{87}$$

to satisfy in order to achieve a second order achromat, which, in general, requires 6 independent sextupole families.

Note that, in analogy with (66), first and second order terms of the arc map can be represented in the form of a single Lie exponent

$$: \mathcal{M}_{arc} : =_2 \; \exp(: \mathcal{Q}_3(x - 0.5 \cdot \bar{r}_{16} \cdot \varepsilon,\, p_x - 0.5 \cdot \bar{r}_{26} \cdot \varepsilon,\, y,\, p_y,\, \varepsilon) \;+\; \bar{r}_{56} \cdot \varepsilon^2 :) \,. \tag{88}$$

C.3 Second Order Aberrations as Integrals of First-Order Trajectories

Let $l_{\mathcal{H}}$ be the length of the half of the arc. Expressing nonzero coefficients of the polynomial $\mathcal{Q}_3$ (second-order chromatic aberrations) as integrals of the first-order trajectories and of the magnetic field parameters we obtain

$$c_{20001}(\mathcal{Q}_3) \;=\; -\int_0^{l_{\mathcal{H}}} \Big(k_2 \bar{r}_{11}^2 \bar{D}_0 \;+\; h \left(\bar{r}_{11}^2\right)' \bar{D}_0' \;+\; h \bar{r}_{21}^2 \bar{D}_0 \;-$$

$$\left(h' \bar{r}_{11}^2 \bar{D}_0\right)' \;+\; 2hk_1 \bar{r}_{11}^2 \bar{D}_0 \;-\; \bar{r}_{21}^2 \Big)\, d\tau \;=$$

$$-\int_0^{l_{\mathcal{H}}} \Big(k_2 \bar{r}_{11}^2 \bar{D}_0 \;+\; h \left(\bar{r}_{11}^2\right)' \bar{D}_0' \;+\; h \bar{r}_{21}^2 \bar{D}_0 \;+\; 2hk_1 \bar{r}_{11}^2 \bar{D}_0 \;-\; \bar{r}_{21}^2 \Big)\, d\tau\,, \tag{89}$$

$$c_{02001}(\mathcal{Q}_3) \;=\; -\int_0^{l_{\mathcal{H}}} \Big(k_2 \bar{r}_{12}^2 \bar{D}_0 \;+\; h \left(\bar{r}_{12}^2\right)' \bar{D}_0' \;+\; h \bar{r}_{22}^2 \bar{D}_0 \;-$$

$$\left(h' \bar{r}_{12}^2 \bar{D}_0\right)' \;+\; 2hk_1 \bar{r}_{12}^2 \bar{D}_0 \;-\; \bar{r}_{22}^2 \Big)\, d\tau \;=$$

$$-\int_0^{l_{\mathcal{H}}} \Big(k_2 \bar{r}_{12}^2 \bar{D}_0 \;+\; h \left(\bar{r}_{12}^2\right)' \bar{D}_0' \;+\; h \bar{r}_{22}^2 \bar{D}_0 \;+\; 2hk_1 \bar{r}_{12}^2 \bar{D}_0 \;-\; \bar{r}_{22}^2 \Big)\, d\tau\,, \tag{90}$$

$$c_{11001}(\mathcal{Q}_3) \;=\; -2\int_0^{l_{\mathcal{H}}} \Big(k_2 \bar{r}_{11} \bar{r}_{12} \bar{D}_0 \;+\; h \left(\bar{r}_{11} \bar{r}_{12}\right)' \bar{D}_0' \;+\; h \bar{r}_{21} \bar{r}_{22} \bar{D}_0 \;-$$

$$\left(h' \bar{r}_{11} \bar{r}_{12} \bar{D}_0\right)' \;+\; 2hk_1 \bar{r}_{11} \bar{r}_{12} \bar{D}_0 \;-\; \bar{r}_{21} \bar{r}_{22} \Big)\, d\tau \;=$$

$$-2\int_0^{l_{\mathcal{H}}} \Big(k_2 \bar{r}_{11} \bar{r}_{12} \bar{D}_0 + h \left(\bar{r}_{11} \bar{r}_{12}\right)' \bar{D}_0' + h \bar{r}_{21} \bar{r}_{22} \bar{D}_0 + 2hk_1 \bar{r}_{11} \bar{r}_{12} \bar{D}_0 - \bar{r}_{21} \bar{r}_{22} \Big)\, d\tau\,, \tag{91}$$

$$c_{00201}(\mathcal{Q}_3) \;=\; \int_0^{l_{\mathcal{H}}} \Big(k_2 \bar{r}_{33}^2 \bar{D}_0 \;-\; h \bar{r}_{43}^2 \bar{D}_0 \;-\; h' \bar{r}_{33}^2 \bar{D}_0' \;+\; hk_1 \bar{r}_{33}^2 \bar{D}_0 \;+\; \bar{r}_{43}^2 \Big)\, d\tau\,, \tag{92}$$

$$c_{00021}(\mathcal{Q}_3) \;=\; \int\limits_0^{l_{\mathcal{H}}} \Big(k_2 \bar{r}_{34}^2 \bar{D}_0 \;-\; h \bar{r}_{44}^2 \bar{D}_0 \;-\; h' \bar{r}_{34}^2 \bar{D}_0' \;+\; h k_1 \bar{r}_{34}^2 \bar{D}_0 \;+\; \bar{r}_{44}^2 \Big)\, d\tau \,, \qquad (93)$$

$$c_{00111}(\mathcal{Q}_3) \;=\; 2 \int\limits_0^{l_{\mathcal{H}}} \Big(k_2 \bar{r}_{33} \bar{r}_{34} \bar{D}_0 \;-\; h \bar{r}_{43} \bar{r}_{44} \bar{D}_0 \;-\; h' \bar{r}_{33} \bar{r}_{34} \bar{D}_0' \;+$$

$$h k_1 \bar{r}_{33} \bar{r}_{34} \bar{D}_0 \;+\; \bar{r}_{43} \bar{r}_{44} \Big)\, d\tau \,, \qquad (94)$$

where

$$\bar{D}_0(\tau) \;=\; \frac{\bar{r}_{11}(\tau) \cdot \bar{r}_{16}(l_{\mathcal{H}}) \;+\; \bar{r}_{12}(\tau) \cdot \bar{r}_{26}(l_{\mathcal{H}})}{2} \;+\; \bar{r}_{16}(\tau) \qquad (95)$$

is the solution for the dispersion function which is periodic within half of the arc and

$$\bar{D}_0'(\tau) \;=\; \frac{\bar{r}_{21}(\tau) \cdot \bar{r}_{16}(l_{\mathcal{H}}) \;+\; \bar{r}_{22}(\tau) \cdot \bar{r}_{26}(l_{\mathcal{H}})}{2} \;+\; \bar{r}_{26}(\tau) \qquad (96)$$

is its derivative with respect to variable τ.

Let us assume that the linear optics of the system is set in accordance with the symmetry FRFR, i.e. that the first half of the arc is a two-cell combination consisting of the forward cell followed by its mirror reflected image (reversed cell), and for the forward cell the conditions (50) are satisfied. Then from (36) and (37) it follows that

$$\bar{r}_{12}(\tau), \quad \bar{r}_{21}(\tau), \quad \bar{D}_0(\tau), \quad \bar{r}_{34}(\tau), \quad \bar{r}_{43}(\tau) \qquad (97)$$

are even and

$$\bar{r}_{11}(\tau), \quad \bar{r}_{22}(\tau), \quad \bar{D}_0'(\tau) \quad \bar{r}_{33}(\tau), \quad \bar{r}_{44}(\tau) \qquad (98)$$

are odd functions with respect to the point $\tau \,=\, l_{\mathcal{H}} \,/\, 2 \,=\, l_c$. This allows us to reduce the parts of integrals (89)-(94) which are independent from sextupole settings, to the integration not over the half of the arc, but to the integration over one quarter of the arc and thus to establish the connection between coefficients of the polynomial $\mathcal{K}_3$ in (66) and coefficients of the polynomial $\mathcal{Q}_3$ in (88). Using formulas (72)-(75) and (89)-(94), the fact that $c_{11001}(\mathcal{K}_3) \,=\, c_{00111}(\mathcal{K}_3) \,=\, 0$ and the symmetry conditions (97)-(98) we obtain

$$c_{20001}(\mathcal{Q}_3) \;=\; -\int\limits_0^{l_{\mathcal{H}}} k_2 \bar{r}_{11}^2 \bar{D}_0 d\tau \;+\; c_{20001}(\mathcal{K}_3,\, k_2 \equiv 0)\,, \qquad (99)$$

$$c_{02001}(\mathcal{Q}_3) \;=\; -\int\limits_0^{l_{\mathcal{H}}} k_2 \bar{r}_{12}^2 \bar{D}_0 d\tau \;+\; c_{02001}(\mathcal{K}_3,\, k_2 \equiv 0)\,, \qquad (100)$$

$$c_{11001}(\mathcal{Q}_3) \;=\; -2\int\limits_0^{l_{\mathcal{H}}} k_2\bar{r}_{11}\bar{r}_{12}\bar{D}_0 d\tau\,, \tag{101}$$

$$c_{00201}(\mathcal{Q}_3) \;=\; \int\limits_0^{l_{\mathcal{H}}} k_2\bar{r}_{33}^2\bar{D}_0 d\tau \;+\; c_{00201}(\mathcal{K}_3,\, k_2 \equiv 0)\,, \tag{102}$$

$$c_{00021}(\mathcal{Q}_3) \;=\; -\int\limits_0^{l_{\mathcal{H}}} k_2\bar{r}_{34}^2\bar{D}_0 d\tau \;+\; c_{00021}(\mathcal{K}_3,\, k_2 \equiv 0)\,, \tag{103}$$

$$c_{00111}(\mathcal{Q}_3) \;=\; 2\int\limits_0^{l_{\mathcal{H}}} k_2\bar{r}_{33}\bar{r}_{34}\bar{D}_0 d\tau\,, \tag{104}$$

where the symbols $c_{abcde}(\mathcal{K}_3,\, k_2 \equiv 0)$ mean the corresponding coefficient of the polynomial $\mathcal{K}_3$ calculated for the sextupole field strength equal to zero ($k_2(\tau) \equiv 0$).

If the sextupole field strength will also follow the symmetry FRFR, than according to (99)-(104) and (72)-(75) the polynomials $\mathcal{Q}_3$ and $\mathcal{K}_3$ will coincide as would be expected, and the two-cell approach to the second-order achromat design turns into the four-cell approach based on reflection symmetry.

References

[1] R.Brinkmann, *Private Communication*, November 4, 2004.

[2] V.Balandin, R.Brinkmann and N.Golubeva, *Preliminary Layout of the XFEL Post-Linac Collimation System*, Presentation at the XFEL Project Group Meeting, 15th December 2004.

[3] V.Balandin and N.Golubeva, *XFEL Collimation Section: Possible solutions for the matching section and phase shifter as a function of maximal allowed strength of quadrupoles (with additional possibility of FODO like focusing in the whole section)*, Unpublished Note, February 2006.

[4] V.Balandin, R.Brinkmann and N.Golubeva, *Post-Linac Collimation System for the European XFEL*, FLS 2006 Workshop, May 15-19, Hamburg (2006).

[5] W.Decking, *Requirements for Collimation and Beam Distribution System: Hardware and Geometrical Constraints*, Private Communication, June 2006.

[6] V.Balandin and N.Golubeva, *XFEL Post-Linac Collimation Section. Update of Optics Solution: July 2006*, Unpublished Note, July 2006.

[7] M.Altarelli, R.Brinkmann et al. (ed) *XFEL: European X-Ray Free-Electron Laser Facility - Technical Design Report*, DESY 2006-097, July 2006.

[8] M.Dohlus, *Presentations at the Beam Dynamic Group Meetings*, http://www.desy.de/xfel-beam/index.html, 2006-2007.

[9] V.Balandin and N.Golubeva, *Requirements on Beta-Functions to Provide a Passive Survival of the XFEL Post-Linac Collimators*, Unpublished Note, October 2004.

[10] W.R.Nelson, H.Hirayma, and D.W.O.Rogers, *The EGS4 code system*, SLAC Report 265 (1985).

[11] NLC Post-Linac Collimation Task Force. *New Post-Linac Collimation System for the Next Linear Collider*, LCC-Note-0052, 21-Feb-2001.

[12] S. van der Meer, *Achromatic Beam Optics for Particle Separator*, Report CERN 60-22 (CERN, Geneva, 1960).

[13] K.Steffen, *High Energy Beam Optics*, Wiley-Interscience, New York, 1965.

[14] E.D.Courant, *Impossibility of Achromatic Focusing with Magnetic Quadrupoles and Solenoids*, Particle Accelerators, 1971, Vol. 2, pp. 117-119.

[15] B.W.Montague and F.Ruggiero, *Apochromatic Focusing for Linear Colliders*, CLIC Note 37, May 1987.

[16] V.Balandin, K.Flöttmann, N.Golubeva and M.Körfer, *Studies of the Collimator System for the TTF Phase 2*, TESLA 2003-17, May 2003.

[17] V.Balandin and N.Golubeva, *The TrackFMN Program. User's Reference Manual*, unpublished.

[18] V.Balandin and N.Golubeva, *Hamiltonian Methods for the Study of Polarized Proton Beam Dynamics in Accelerators and Storage Rings*, DESY 98-016, February 1998.

[19] S.Penner, *Calculation of Properties of Magnetic Deflection Systems*, Rev. Sci. Instr. 32 (1961), 150-160.

[20] E.E.Bliamptis, *Reflection Properties of Deflecting Magnet Systems*, Rev. Sci. Instr. 35 (1964), 1521-1522.

[21] J.C.Herrera and E.E.Bliamptis, *Symmetry Properties of Beam Handling Magnet Systems*, Rev. Sci. Instr. 37 (1966), 183-188.

[22] J.McL.Emmerson and N.Middlemas, *Symmetry Properties in Beam Transport Systems*, Nucl. Instr. and Meth. 24 (1963) 93-102.

[23] M.Berz, *Modern Map Methods in Particle Beam Physics*, Academic Press (1999), 318p., (Advances in Imaging and Electron Physics, 108).

[24] G.J.Gardner, *The Vector Potential In Accelerator Magnets*, Part.Accel. 35:215-226, 1991.

[25] A.Dragt, *Lectures on Nonlinear Orbit Dynamics*, AIP Conf.Proc. No. 87, pp. 147-313, 1982.

[26] W.Wan and M.Berz, *Analytical theory of arbitrary-order achromats*, Phys. Rev. E **54**, 2870(1996).

[27] W.Wan, *Theory and Applications of Arbitrary-Order Achromats*, Ph.D. Thesis 1995, Michigan State University.

[28] K.L.Brown, *A Second-Order Magnetic Optical Achromat*, SLAC-PUB-2257, February 1979.

[29] K.L.Brown and R.V.Servranckx, *Applications of the Second-Order Achromat Concept to the Design of Particle Accelerators*, IEEE, Trans.Nucl.Sci. 32:2288, 1985.

[30] S.A.Kheifets, T.H.Fieguth and R.D.Ruth, *Canonical Description of a Second-Order Achromat*, SLAC-PUB-4569, March 1988.

[31] T.H.Fieguth and J.J.Murray, *Design of the SLC Damping Ring to Linac Transport Lines*, SLAC-PUB-3174, July 1983.